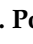





Article

Dramatic Effect of A Ring Size of Alicyclic α -Dioximate Ligand Synthons on Kinetics of the Template Synthesis and of the Acidic Decomposition of the Methylboron-Capped Iron(II) Clathrochelates

Alexander L. Pomadchik ¹, Alexander S. Belov ^{1,2}, Ekaterina G. Lebed ^{1,2}, Irina G. Belaya ¹, Anna V. Vologzhanina ¹ and Yan Z. Voloshin ^{1,2,*}

¹ Nesmeyanov Institute of the Organoelement Compounds of the Russian Academy of Sciences, 119991 Moscow, Russia; pom17@yandex.ru (A.L.P.); as_belov@mail.ru (A.S.B.); lebed@ineos.ac.ru (E.G.L.); mair2005@yandex.ru (I.G.B.); vologzhanina@mail.ru (A.V.V.)

² Kurnakov Institute of General and Inorganic Chemistry of the Russian Academy of Sciences, 119991 Moscow, Russia

* Correspondence: voloshin@ineos.ac.ru or voloshin@igic.ras.ru



Citation: Pomadchik, A.L.; Belov, A.S.; Lebed, E.G.; Belaya, I.G.; Vologzhanina, A.V.; Voloshin, Y.Z. Dramatic Effect of A Ring Size of Alicyclic α -Dioximate Ligand Synthons on Kinetics of the Template Synthesis and of the Acidic Decomposition of the Methylboron-Capped Iron(II) Clathrochelates. *Molecules* **2021**, *26*, 4019. <https://doi.org/10.3390/molecules26134019>

Academic Editors: Girolamo Casella and Silvia Carlotto

Received: 18 May 2021
Accepted: 27 June 2021
Published: 30 June 2021

Publisher's Note: MDPI stays neutral with regard to jurisdictional claims in published maps and institutional affiliations.



Copyright: © 2021 by the authors. Licensee MDPI, Basel, Switzerland. This article is an open access article distributed under the terms and conditions of the Creative Commons Attribution (CC BY) license (<https://creativecommons.org/licenses/by/4.0/>).

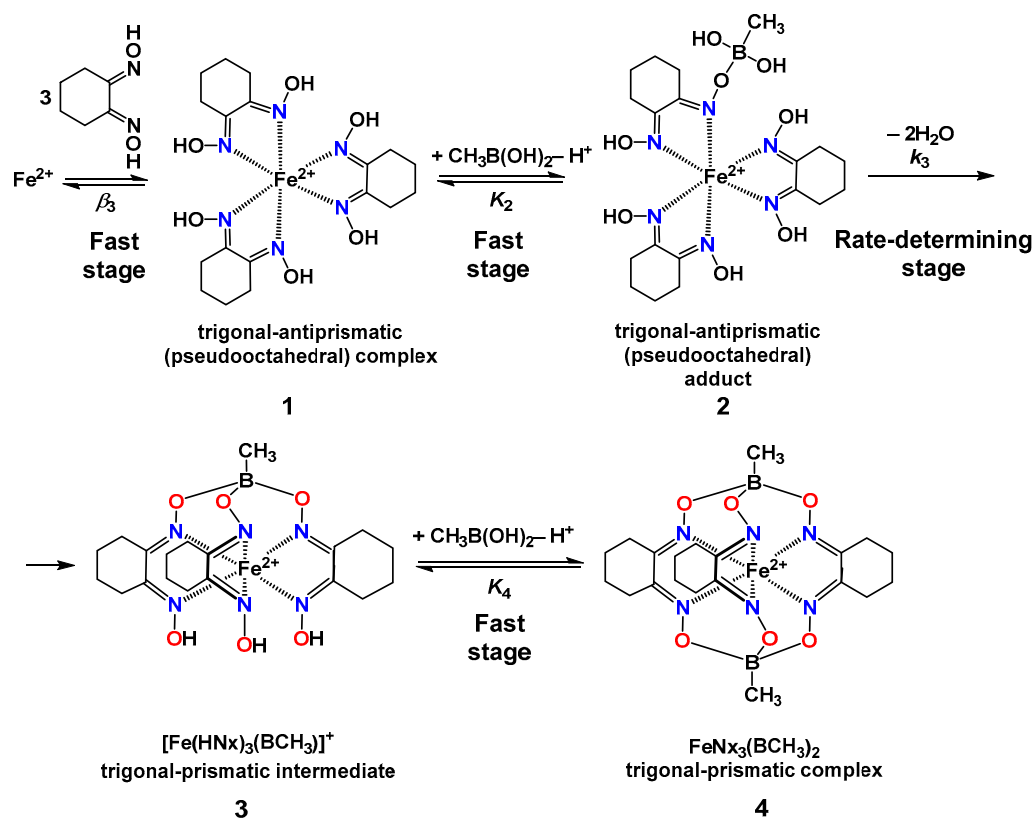
Abstract: Kinetics and thermodynamics of the template synthesis and of the acidic decomposition of the methylboron-capped iron(II) tris-1,2-dioximates—the clathrochelate derivatives of six (nioxime)- and eight (octoxime)-membered alicyclic ligand synthons—were compared. In the case of a macrobicyclic iron(II) tris-nioximate, the plausible pathway of its formation contains a rate-determining stage and includes a reversible formation of an almost trigonal-antiprismatic (TAP) protonated tris-complex, followed by its monodeprotonation and addition of $\text{CH}_3\text{B}(\text{OH})_2$. Thus, the formed TAP intermediate undergoes a multistep rate-determining stage of double cyclization with the elimination of two water molecules accompanied by a structural rearrangement, thus giving an almost trigonal-prismatic (TP) iron(II) semiclatrochelate. It easily undergoes a cross-linking with $\text{CH}_3\text{B}(\text{OH})_2$, resulting in the elimination of H^+ ion and in the formation of a macrobicyclic structure. In contrast, the analogous scheme for its macrobicyclic tris-octoximate analog was found to contain up to three initial stages affecting the overall synthesis reaction rate. The rates of acidic decomposition of the above clathrochelates were found to be also affected by the nature of their ribbed substituents. Therefore, the single crystal XRD experiments were performed in order to explain these results. The difference in the kinetic schemes of a formation of the boron-capped iron(II) tris-nioximates and tris-octoximates is explained by necessity of the substantial changes in a geometry of the latter ligand synthon, caused by its coordination to the iron(II) ion, due to both the higher distortion of the FeN_6 -coordination polyhedra, and the intramolecular sterical clashes in the molecules of the macrobicyclic iron(II) tris-octoximates.

Keywords: macrocyclic compounds; cage complexes; clathrochelates; iron complexes; template synthesis; acidic decomposition; kinetics of complexation; thermodynamics of complexation; X-ray diffraction

1. Introduction

Reactions of the template synthesis of the boron-capped iron(II) cage complexes (clathrochelates [1,2]), the derivatives of six-, seven- and eight-membered alicyclic dioximes, are known [1,3–6] to be the unique objects thanks to experimental studies carried out on them. Indeed, the above clathrochelates quantitatively form in the diluted aqueous and/or aqueous–organic solutions in a wide range of the corresponding semiconversion reaction times, thus allowing their photometrical detection using the characteristic of this type of the quasaromatic polyazomethine complexes intensive metal-to-ligand charge transfer (MLCT) $\text{Fed} \rightarrow \text{L}\pi^*$ bands in the visible range with maxima at approximately 450 nm. Such experimental conditions seem to be more beneficial than those known from

the literature [7–14] for their oximate and amine analogs. Recently, we performed [6] a detailed study of the kinetics and thermodynamics of both the template synthesis and the acidic decomposition of the macrobicyclic iron(II) tris-cyclohexanedion-1,2-dioximate (nioximate, Nx^{2-}) $\text{FeN}\text{x}_3(\text{BCH}_3)_2$ that is formed by a cross-linking with methylboronic acid. The proposed [6] pathway of its formation shown in Scheme 1 contains a multistep rate-determining stage and includes a reversible and fast formation of the protonated non-macrocyclic iron(II) tris-nioximate, possessing an almost TAP geometry with the TP–TAP distortion angle φ close to 60° (the φ value for an ideal TP is equal to 0° and that for an ideal TAP is equal to 60°). This first stage is so fast that the values of the corresponding direct k_1 and reverse k_{-1} kinetic constants ($\beta_3 = k_1/k_{-1}$) could not be obtained. It is followed by the monodeprotonation of **1** and the addition of the first molecule of $\text{CH}_3\text{B}(\text{OH})_2$, giving the adduct **2**. The TAP intermediate obtained in this way undergoes a rate-determining stage of double cyclization with the elimination of two water molecules and an additional structural TAP \rightarrow TP rearrangement. This gives a TP semiclatrochelate **3** that easily undergoes a cross-linking with the second molecule of $\text{CH}_3\text{B}(\text{OH})_2$, resulting in the elimination of H^+ ion and in the formation of the tris-nioximate iron(II) clathrochelate molecule **4** with two methylboron capping fragments [6]. In the present paper, we report the preparation of a new macrobicyclic iron(II) tris- α -dioximate; the derivative of an eight-membered alicyclic ligand synthon {cyclooctanedion-1,2 dioxime (octoxime), H_2Ox } and the single crystal X-ray diffraction structures of this complex and also its above tris-cyclohexane-containing analog. We found a dramatic effect of the nature of an initial alicyclic α -dioxime on the kinetics and thermodynamics of both the template synthesis and the acidic decomposition of cage complexes under study.



Scheme 1. Most plausible pathway of a formation of the clathrochelate $\text{FeN}\text{x}_3(\text{BCH}_3)_2$. Adapted from [6].

$$\frac{dc}{dt} = k_3[Fe(H_2Nx)_2(HNx) \cdot CH_3B(OH)_2]^+ = k_3K_2\beta_3[Fe^{2+}][H_2Nx]^3[CH_3B(OH)_2][H^+]^{-1}$$

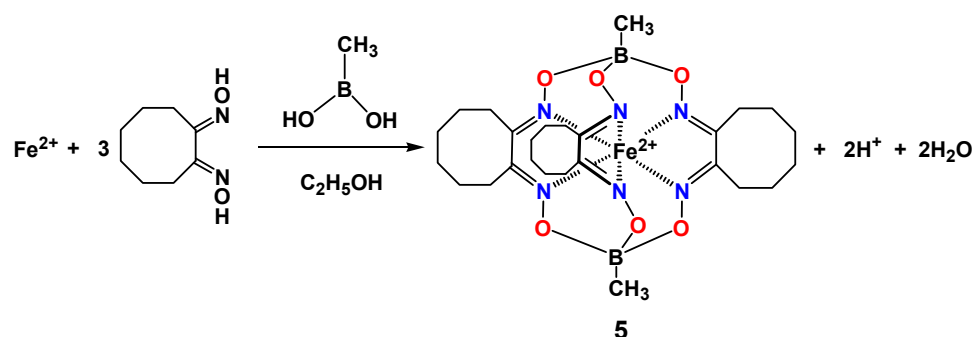
$$k_s = k_3K_2\beta_3 \quad (1)$$

These changes in their parameters were explained using the obtained XRD data for them and those for their initial α -dioximate ligand synthons and clathrochelate analogs with known XRD structures.

2. Results and Discussion

2.1. Synthesis and Spectra

Clathrochelate $FeOx_3(BCH_3)_2$ (5) was obtained in a moderate yield of 65% by Scheme 2 under mild reaction conditions (i.e., at room temperature with ethanol as a solvent) using the template condensation of octoxime and methylboronic acid on the iron(II) ion as a matrix.



Scheme 2. Preparation of the complex $FeOx_3(BCH_3)_2$ (5).

The prepared new iron(II) cage complex was characterized using elemental analysis, MALDI-TOF mass spectrometry, UV-Vis, 1H and $^{13}C\{^1H\}$ NMR spectra, as well as by the single crystal X-ray diffraction (see below). We also performed the analogous XRD experiment of its earlier-described [6] tris-nioximate analog $FeNx_3(BCH_3)_2$ (4).

The diamagnetic character of these TP-TAP cage complexes, which have the low-spin d^6 electronic configuration of their encapsulated metal ion, is clearly seen from the NMR and XRD experiments (see below), as well as from the literature data [1,15–18] on ^{57}Fe Mössbauer spectra for more than hundred iron(II) macrobicyclic tris- α -dioximates and tris-oximehydrazonates. Their three bonding $t_{2g} \rightarrow e_1 + a_1$ orbitals are fully occupied [19–25] due to a very high ligand field strength, characteristic of a given type of the caging ligands. The experimentally observed increase in ligand field strength (as compared with the corresponding non-macrocyclic iron(II) tris- α -dioximates) can be due to the so-called “macrocyclic effect” that is caused by a formation of their quasiaromatic macrobicyclic polyazomethine frameworks [1]. As a result, all these iron(II) cage complexes (such as the well-known pseudooctahedral, possessing an almost TAP geometry, iron(II) trisphenanthrolinates and tris- α -bipyridinates [21,22,26–28]) are the low-spin diamagnetic compounds in their ground states.

The most intense peak in the positive range of MALDI-TOF mass spectrum of the clathrochelate $FeOx_3(BCH_3)_2$ (5, see Supplementary Materials, Figure S8) belongs to its molecular ion. The number and positions of the signals in its solution 1H and $^{13}C\{^1H\}$ NMR spectra (see Supplementary Materials, Figures S9 and S10), as well as the ratios of their integral intensities in its 1H NMR spectrum (in particular, those of the signals of the apical methyl protons and of the α -, β - and γ -methylene protons of the ribbed eight-membered alicycles) confirmed the composition and C_3 -symmetry of the molecule $FeOx_3(BCH_3)_2$ (5). It should also be noted that the signals of methylene protons in the solution 1H NMR spectra of the macrobicyclic complexes under discussion appeared in their spectra as broadened singlets (except that of α -methylene groups of new methylboron-

capped iron(II) tris-octoximate, which appeared in its spectrum as a triplet) because their unsubstituted alicyclic fragments undergo a very fast exchange (in the NMR time scale at given experimental conditions) between their possible conformations. It should be noted that in the solution NMR spectra of more than hundred iron(II) clathrochelates—the derivatives of unsubstituted six-, seven- and eight-membered alicyclic α -dioximes, which have been prepared to date [1,2], we never observed a fine structure of the signals of protons of their α -, β - and γ -methylene groups, caused by the intramolecular ^1H - ^1H interactions (except for those of α -methylene protons of the alkylboron-capped iron(II) eight-membered alicyclic α -dioximates). The above NMR spectra also suggest a diamagnetic character of new iron(II) complex $\text{FeOx}_3(\text{BCH}_3)_2$ (5) (no paramagnetic shifts or paramagnetic broadenings of its NMR signals are observed). The number of lines in its $^{13}\text{C}\{^1\text{H}\}$ NMR spectrum also confirmed an equivalence of ribbed chelating α -dioximate fragments of its macrobicyclic molecule.

UV-vis spectrum of the methylboron-capped tris-octoximate $\text{FeOx}_3(\text{BCH}_3)_2$ (5) (Figure 1), measured from its solution in dichloromethane, contains in its visible range one intense ($\varepsilon \sim 2.6 \times 10^4 \text{ mol}^{-1} \text{ L cm}^{-1}$) asymmetric MLCT $\text{Fe}d \rightarrow L\pi^*$ band with maximum at approximately 450 nm.

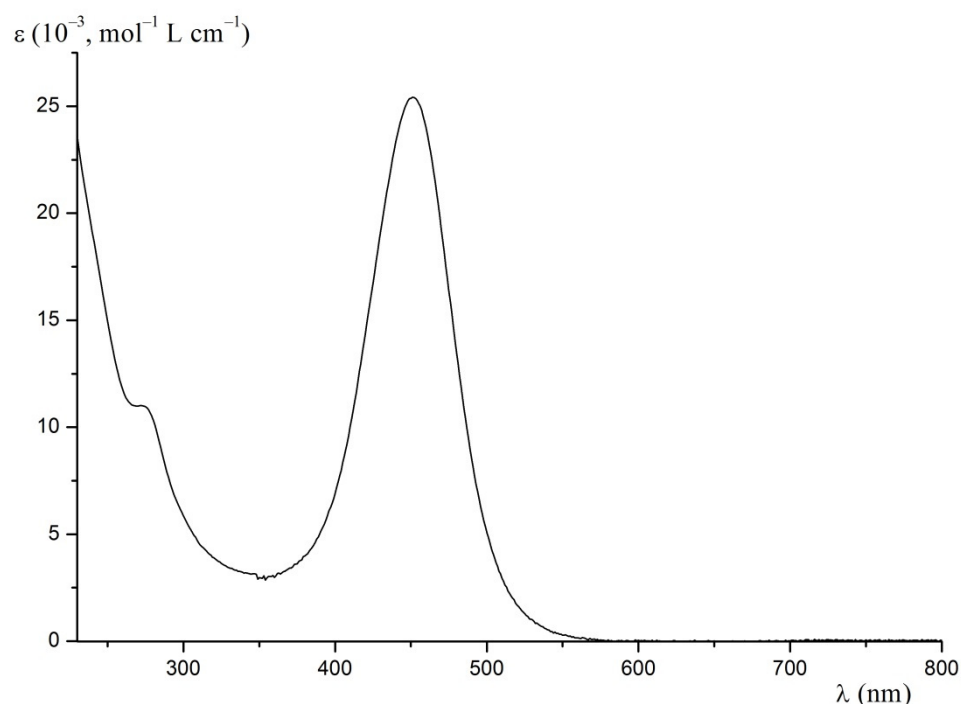


Figure 1. The solution UV-vis spectrum of the complex $\text{FeOx}_3(\text{BCH}_3)_2$ (5) in dichloromethane at its concentration equal to $2.1 \times 10^{-4} \text{ mol L}^{-1}$.

2.2. Kinetics of the Template Synthesis of $\text{FeOx}_3(\text{BCH}_3)_2$

Overall kinetic equation of the formation of this iron(II) cage complex (Scheme 2) can be described by Equation (2):

$$\frac{dc}{dt} = k_s \cdot [\text{Fe}^{2+}]^j \cdot [\text{H}_2\text{Ox}]^m \cdot [\text{CH}_3\text{B}(\text{OH})_2]^n \cdot [\text{H}^+]^p \quad (2)$$

At low concentrations of the iron(II) ions and a great excess of other reaction components (this suggests that the changes in their concentrations are negligible), this equation can be rewritten as:

$$\frac{dc}{dt} = k_{eff}^s \cdot [\text{Fe}^{2+}]^j \quad (3)$$

where $k_{eff}^s = k_s \cdot [H_2Ox]^m \cdot [CH_3B(OH)_2]^n \cdot [H^+]^p$.

So, it is possible to obtain an order with respect to the concentration of Fe^{2+} ions using a plot of the initial synthesis reaction rates dc/dt versus their concentration. Optical density A at a given wavelength after a given time interval is related to the concentration of the resulting clathrochelate $FeOx_3(BCH_3)_2$ (5) by the classical equation: $A = \epsilon l c$ (where ϵ is the molar extinction coefficient of this complex, c is its molar concentration and l is the light path). Therefore, it is possible to use the dA/dt values as the characteristics of a synthesis reaction rate (Figure 2) and a set of the obtained experimental data can be described as the first-order kinetics (Equation (3)) with respect to the concentration of Fe^{2+} ions (see the plot of $\log(dA/dt)$ versus $\log[Fe^{2+}]$ shown in Figure 3).

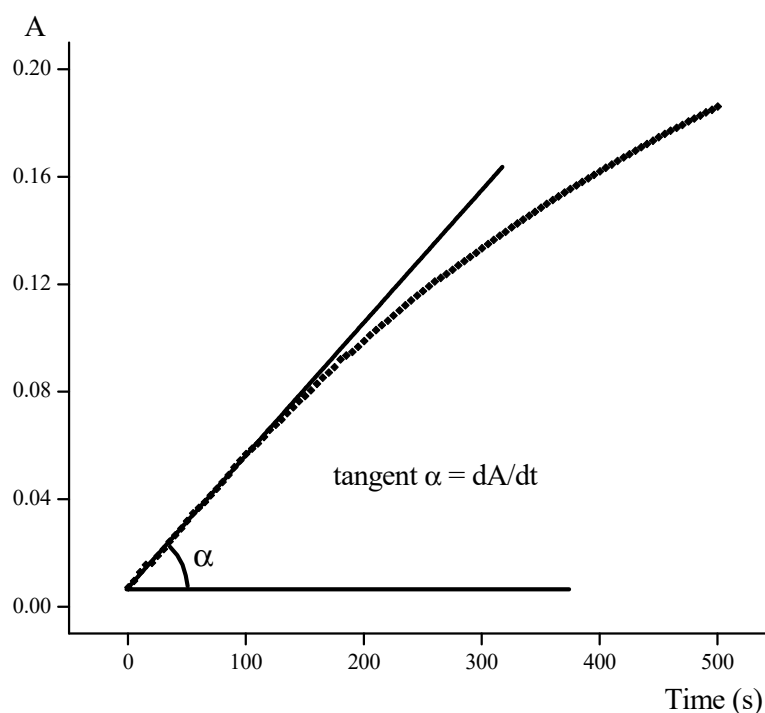


Figure 2. Example of a determination of the initial synthesis reaction rate dA/dt for the complex $FeOx_3(BCH_3)_2$ (5) at $[Fe^{2+}] = 2 \times 10^{-5} \text{ mol L}^{-1}$, $[H_2Ox] = 1.5 \times 10^{-3} \text{ mol L}^{-1}$, $[CH_3B(OH)_2] = 5 \times 10^{-3} \text{ mol L}^{-1}$ and $pH = 3.75$.

Thus, the effective synthesis rate constant k_{eff}^s at the low concentrations of Fe^{2+} ions was determined as a pseudo-first-order rate constant [29] using the following Equation (4):

$$\ln \frac{A_{max}}{A_{max} - A} = k_{eff}^s \cdot t \quad (4)$$

where A_{max} is the maximal optical density that corresponds to a complete binding of Fe^{2+} ions caused by the formation of the complex $FeOx_3(BCH_3)_2$ (5).

Then the reaction orders with respect to the concentrations (or an activity in the case of the realizing H^+ ions) of other components (H_2Ox , $CH_3B(OH)_2$ and H^+) were studied using the k_{eff}^s values obtained as a slope of the corresponding linear regression, as shown in Figure 4.

To obtain a reaction order with respect to the concentration of a given component, its value has been changed in a relatively wide range, whereas the concentrations of other components persist. In the case of H^+ ions, we suggested that in the diluted solutions, which were used for the kinetic experiments on the formation of a cage complex under study, the concentration of H^+ ions could be assumed equal to their activity a_{H^+} . The latter value was measured using an appropriate pH-meter equipped with a given working

pH-electrode (see the Experimental part). We suggested to obtain a reaction order with respect to the concentration of each of these components as the tangent of a linear regression plotted in the coordinates $\log k_{eff}^s$ versus $\log c_{comp}$. Indeed, as it can be seen from Figure 5, such an order with respect to the concentration of octoxime is equal to 3. It was also found that at pa_{H^+} values higher than approximately 3.8, the optical densities A of the solutions under study substantially increase, even in the absence of methylboronic acid. This effect is probably caused by the formation of the non-macrocyclic iron(II) mono- and bis- α -dioximates; the derivatives of a monodeprotonated form of octoxime (i.e., the HOx^- monoanion). Below this pa_{H^+} value, the synthesis reaction order with respect to the activity of H^+ ions is equal to -1 (Figure 6). On the other hand, in general, the corresponding plots versus the concentration of methylboronic acid (Figure 7) are not the linear regressions, but such a plot can adopt its linear form at the selected experimental conditions (first of all, at the appropriate concentrations of other components).

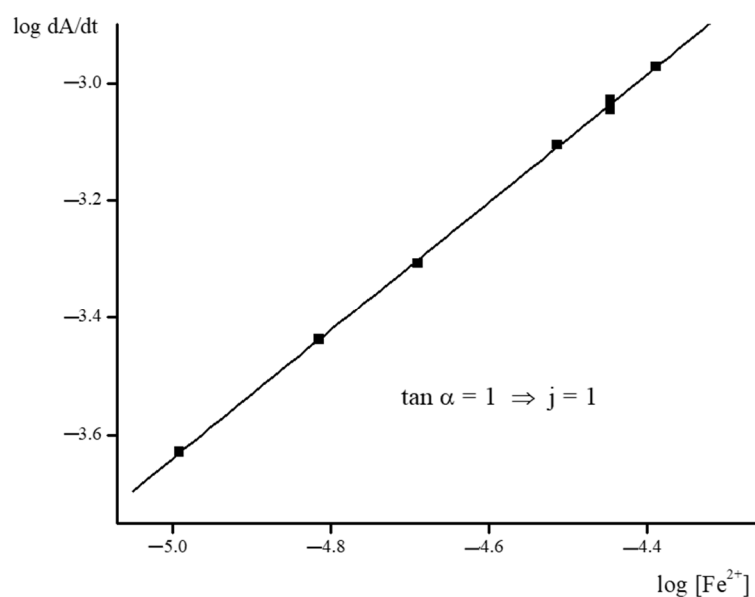


Figure 3. Determination of the synthesis reaction order for the complex $FeOx_3(BCH_3)_2$ (5) with respect to the concentration of Fe^{2+} ions at $[H_2Ox] = 1.5 \times 10^{-3} \text{ mol L}^{-1}$, $[CH_3B(OH)_2] = 5 \times 10^{-3} \text{ mol L}^{-1}$ and $pH = 3.75$.

A similar result has been previously observed [3] in the case of the hydroxyboron-capped macrobicyclic iron(II) tris-octoximate $FeOx_3(BOH)_2$. Indeed, the rates of two first stages of its formation are reported in this work to be comparable with that of a structural TAP \rightarrow TP rearrangement, which is the rate-determining stage for other iron(II) clathrochelates of this type (Scheme 1). So, the Equations (5)–(7) describing three consecutive processes, the initial two of which are reversible, have been evaluated [3]. The rates of these intermediate stages have been assumed to be equal (i.e., the concentrations of the corresponding complex intermediates in the proposed [3] scheme of the formation of clathrochelate $FeOx_3(BOH)_2$ persist):

$$dc/dt = k_1[Fe^{2+}][H_2Ox]^3 - k_{-1}[Fe(H_2Ox)_3^{2+}] \quad (5)$$

$$dc/dt = k_2[Fe(H_2Ox)_3^{2+}][H_3BO_3] - k_{-2}[Fe(H_2Ox)_2(HOx) \cdot B(OH)_3^+][H^+] \quad (6)$$

$$dc/dt = k_3[Fe(H_2Ox)_2(HOx) \cdot B(OH)_3^+] \quad (7)$$

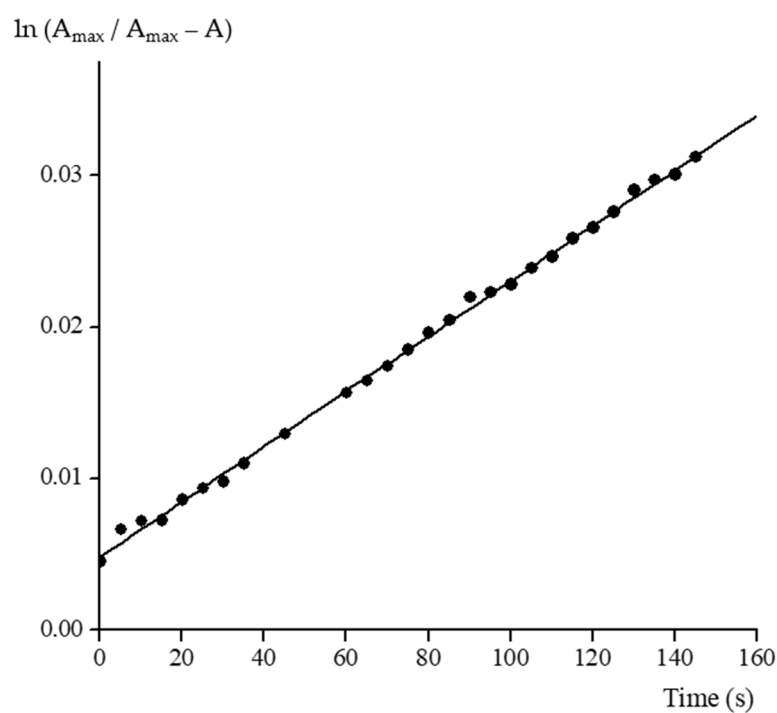


Figure 4. Example of an experimental determination of the synthesis reaction rate constant k_{eff}^s for the complex $\text{FeOx}_3(\text{BCH}_3)_2$ (5) at $[\text{Fe}^{2+}] = 2 \times 10^{-5} \text{ mol L}^{-1}$, $[\text{H}_2\text{Ox}] = 1.5 \times 10^{-3} \text{ mol L}^{-1}$, $[\text{CH}_3\text{B}(\text{OH})_2] = 5 \times 10^{-3} \text{ mol L}^{-1}$ and $\text{pH} = 3.75$.

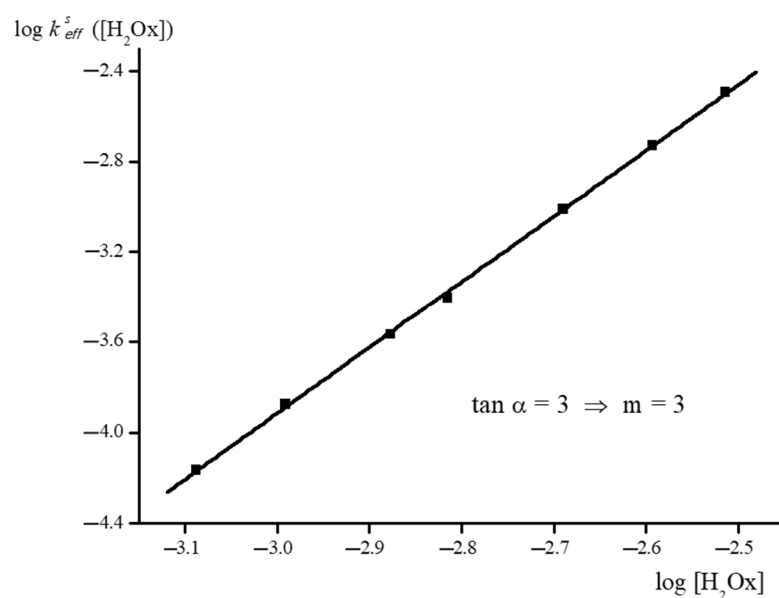


Figure 5. Determination of an order of the synthesis reaction rate constant k_{eff}^s for the complex $\text{FeOx}_3(\text{BCH}_3)_2$ (5) with respect to the concentration of octoxime at $[\text{Fe}^{2+}] = 1.5 \times 10^{-5} \text{ mol L}^{-1}$, $[\text{CH}_3\text{B}(\text{OH})_2] = 5 \times 10^{-3} \text{ mol L}^{-1}$ and $\text{pH} = 3.3$.

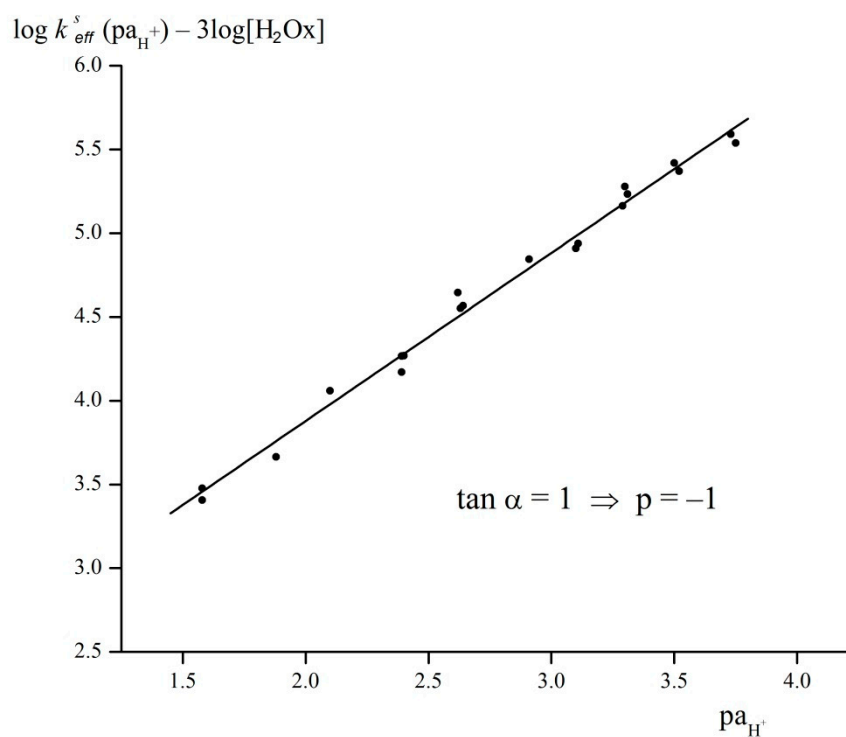


Figure 6. Plot of $\log k_{eff}^s(pa_{H^+}) - 3 \log[H_2Ox]$ versus pa_{H^+} for the complex $FeOx_3(BCH_3)_2$ (5) at $[Fe^{2+}] = 2.5 \times 10^{-5} \text{ mol L}^{-1}$ and $[CH_3B(OH)_2] = 1 \times 10^{-2} \text{ mol L}^{-1}$.

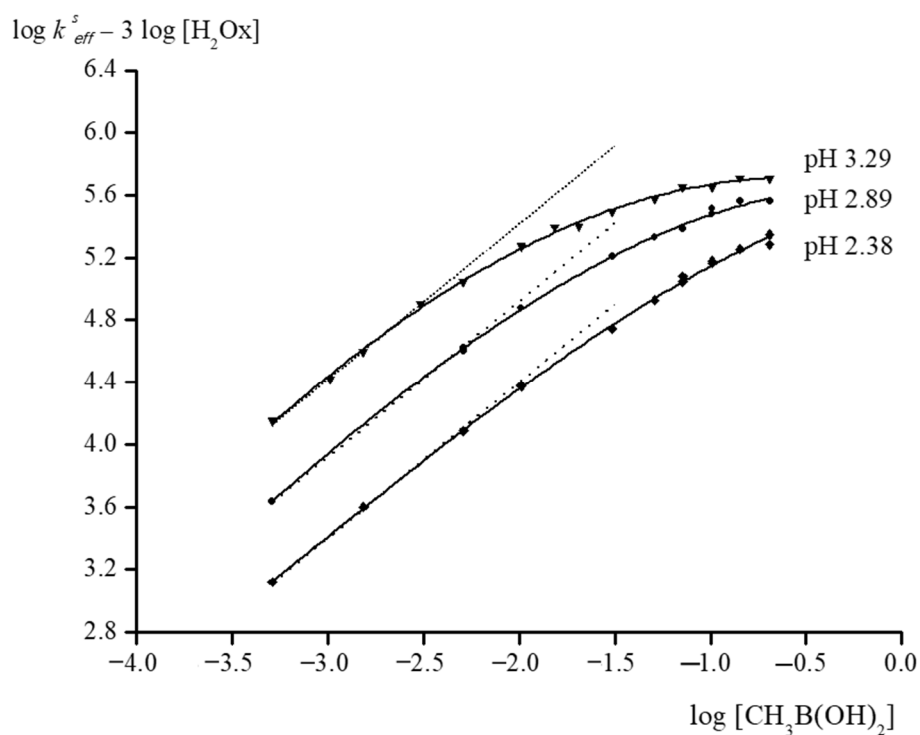


Figure 7. Plots of $\log k_{eff}^s - 3 \log[H_2Ox]$ versus $\log[CH_3B(OH)_2]$ at the different pH values and various concentrations of Fe^{2+} ions and of octoxime.

Solving these equations relative to the synthesis reaction rate, the following Equation (8), which is in good agreement with the obtained [3] experimental data, has been evaluated in that work:

$$dc/dt = \frac{k_3 k_1 k_2 [Fe^{2+}] [H_2Ox]^3 [H_3BO_3]}{k_{-1} k_3 + k_3 k_2 [H_3BO_3] + k_{-1} k_{-2} [H^+]} \quad (8)$$

So, the analogous Equations (9)–(12) we used for evaluation of the obtained experimental results on a template assembling of the molecule $FeOx_3(BCH_3)_2$ (5).

$$dc/dt = k_1 [Fe^{2+}] [H_2Ox]^3 - k_{-1} [Fe(H_2Ox)_3]^{2+} \quad (9)$$

$$dc/dt = k_2 [Fe(H_2Ox)_3]^{2+} [CH_3B(OH)_2] - k_{-2} [Fe(H_2Ox)_2(HOx) \cdot CH_3B(OH)_2^+] [H^+] \quad (10)$$

$$dc/dt = k_3 [Fe(H_2Ox)_2(HOx) \cdot CH_3B(OH)_2^+] \quad (11)$$

$$dc/dt = \frac{k_3 k_1 k_2 [Fe^{2+}] [H_2Ox]^3 [CH_3B(OH)_2]}{k_{-1} k_3 + k_3 k_2 [CH_3B(OH)_2] + k_{-1} k_{-2} [H^+]} \quad (12)$$

The calculated ratios of the synthesis reaction rate constants for the complex $FeOx_3(BCH_3)_2$ (5) thus allowed us to obtain the values of some constants in Equation (12) (in particular, those of the direct complexation $Fe^{2+} + 3H_2Ox \rightarrow [Fe(H_2Ox)_3]^{2+}$ (k_1) and a reverse decomplexation $[Fe(H_2Ox)_3]^{2+} \rightarrow Fe^{2+} + 3H_2Ox$ (k_{-1}) processes). For this purpose, we also used the initially experimentally obtained [3] value of the stability constant β_3 for a given protonated non-macrocyclic iron(II) tris-octoximate **6**. To obtain values of those of the ratios, which are compiled in Table 1, Equation (12) was transformed into the following form:

$$\frac{[H_2Ox]^3}{k_{eff}^s} = \frac{k_{-1}}{k_1 k_2} \left(1 + \frac{k_{-2}}{k_3} [H^+]\right) \frac{1}{[CH_3B(OH)_2]} + \frac{1}{k_1} \quad (13)$$

Table 1. Kinetic and thermodynamic parameters of the template synthesis and the acidic decomposition reactions of the methylboron-capped iron(II) tris-octoximate $FeOx_3(BCH_3)_2$ (5), and those for its tris-nioximate (4) [6] and hydroxy-, phenyl- and *n*-butylboron-capped tris-octoximate [1] analogs.

Complex	^b $\log \beta_3$	k_s $s^{-1} L^3 mol^{-3}$	$k_1 \times 10^{-5}$ $s^{-1} L^3 mol^{-3}$	k_{-1} s^{-1}	k_2 $s^{-1} L mol^{-1}$	k_{-2}/k_3	k_{-3} $s^{-1} L^2 mol^{-2}$	^c K_4	K_5	$k_6 \times 10^5$ $s^{-1} L^2 mol^{-2}$	k_{-6} $s^{-1} L^2 mol^{-2}$
^a $FeOx_3(BCH_3)_2$	^b 5.37		4.36 (pH2.38) 5.73 (pH3.18) 6.78 (pH3.75)	1.86 (pH2.38) 2.45 (pH3.18) 2.89 (pH3.75)	343 (pH2.38) 451 (pH3.18) 533 (pH3.75)	8960					
$FeOx_3(BOH)_2$	^b 5.37		0.445	0.19	22	424	0.12	129			
$FeOx_3(BC_6H_5)_2$		1.2×10^4					0.09	292	240	5.0	3.5
$FeOx_3(Bn-C_4H_9)_2$		2.1×10^4					0.11	147	129	31.1	5.9
$FeNx_3(BCH_3)_2$	^b 4.94	3.2×10^3									

^a This work. ^b β_3 is an earlier obtained [1] stability constant for the corresponding non-macrocyclic tris-dioximate $[Fe(H_2D)_3]^{2+}$ measured [1] in aqueous solutions. ^c $K_4 = K_5^{-1} K_6^{-1}$.

Then, on the first stage of evaluation of Equation (13), we plotted the linear regressions of $[H_2Ox]^3/k_{eff}^s$ versus $1/[CH_3B(OH)_2]$ at various pH values (see Supplementary Materials, Figure S1), thus obtaining the values of $1/k_1$ as the corresponding Y-intercepts. The slopes of these linear regressions were used on the next stage of the experimental data treatment for obtaining of the k_{-1}/k_2 and k_{-2}/k_3 ratios from the corresponding linear regression versus the activity of H^+ ions shown in Figure S3 (see Supplementary Materials) as its slope and its Y-intercept, respectively. It should be noted that values of k_1 obtained in this way depend on the activity of H^+ ions (see Supplementary Materials, Figure S2). This result can be explained by an increase in both an ionic strength (up to $9 \times 10^{-3} mol L^{-1}$ at pH 2.38) and a dielectric constant. These two factors are known from the literature to substantially change the thermodynamic activities of polycharged inorganic and complex

ions (in particular, those of the doubly charged metal cations). Therefore, they could also have an impact on the corresponding kinetic constants. Trying to take account of these effects in our further evaluation of the experimental data, the slopes of linear regressions versus $1/[\text{CH}_3\text{B}(\text{OH})_2]$ (see Supplementary Materials, Figure S1), which were plotted on the above first step, we corrected on the second step of our calculations by dividing them by the values of the corresponding Y-intercepts. The plotted linear regression shown in Figure S3 (see Supplementary Materials) is well fitted to the obtained experimental data, which suggests that the amounts of both the above parameters (i.e., an ionic strength and a dielectric constant) in the solutions under study were precisely taken into account.

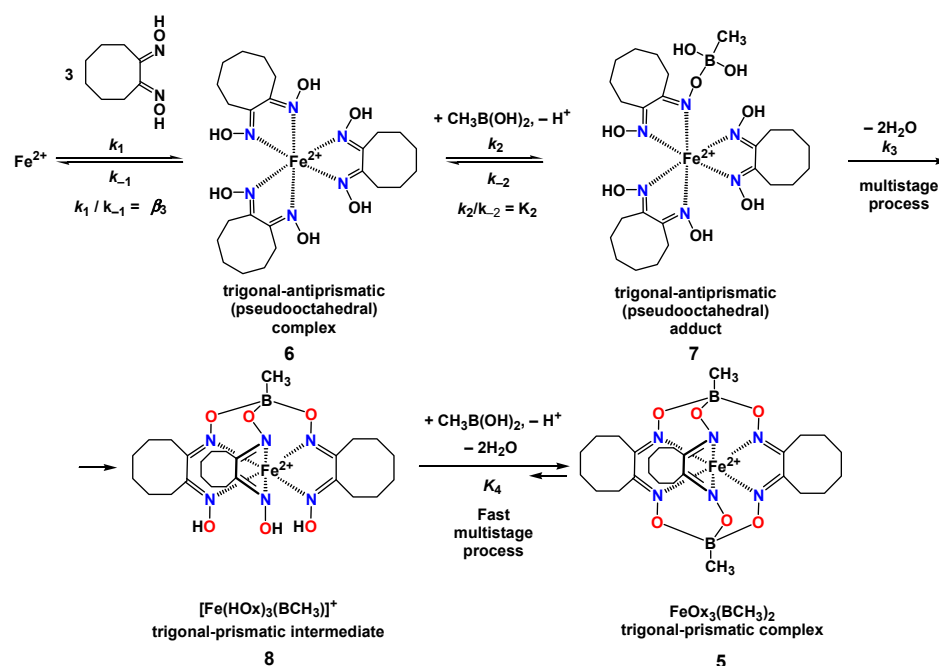
The $k_{-1}k_{-2}[\text{H}^+]$ value is much higher than that of $k_{-1}k_3 + k_3k_2[\text{CH}_3\text{B}(\text{OH})_2]$ in a wide range of the component's concentrations and molar ratios. Therefore, Equation (12) assumes the regular for a given type of the boron-capped alicyclic iron(II) tris- α -dioximates form of Equation (14):

$$dc/dt = k_{eff}^s[\text{Fe}^{2+}][\text{H}_2\text{D}]^3[\text{RB}(\text{OH})_2][\text{H}^+]^{-1} \quad (14)$$

In particular, this equation is reported [5] to describe the synthesis reaction rate constants for the organoboron-capped tris-octoximate complexes $\text{FeOx}_3(\text{BC}_6\text{H}_5)_2$ and $\text{FeOx}_3(\text{B}n\text{-C}_4\text{H}_9)_2$. The observed changes of the kinetic schemes and thermodynamic parameters in a passing from the hydroxyboron-capped iron(II) tris-octoximate to its *n*-butyl- and phenylboron-cross-linked macrobicyclic analogs have been explained [5] by a substantial decrease in the rate constant k_{-2} of a reverse detachment reaction of a molecule of the corresponding organoboron Lewis acid. This results in an increase in the corresponding equilibrium constant K_2 and, therefore, in the synthesis reaction rate constant k_s as well (see Scheme 1 and Equation (1)). As a result, if the plausible scheme of a formation of the hydroxyboron-cross-linked complex $\text{FeOx}_3(\text{BOH})_2$ contains at least two or three stages possessing the similar rates and thus affecting the overall synthesis reaction rate. In contrast, those for its above organoboron-capped analogs contain a rate-determining stage in the used ranges of their component's concentrations.

Similar deductions can be pointed out for explanation of the unexpected plots describing the experimental data on the synthesis reaction of the methylboron-capped macrobicyclic tris-octoximate $\text{FeOx}_3(\text{BCH}_3)_2$ (5). Therefore, the plausible pathway of its formation shown in Scheme 3 can be evaluated. It includes a reversible formation of the protonated non-macrocyclic tris-octoximate dication $[\text{Fe}(\text{H}_2\text{Ox})_3]^{2+}$ (6), followed by a monodeprotonation of this TAP complex and by an addition of one molecule of methylboronic acid (or alternatively, vice versa, a deprotonation of $\text{CH}_3\text{B}(\text{OH})_2$ and, then, an addition of its anionic form to 6 may take place), thus giving a TAP adduct 7. Then, most probably, this adduct undergoes a double cyclization with the elimination of two water molecules to form the monocapped TP semiclatrochelate monocation 8. A more detailed mechanism of this clearly multistage process may include, alternatively, a formation of the corresponding boronic hemiester on its second stage, and then, either a deprotonation of one oxime group of 7—followed by its coordination to the Lewis-acidic boron atom possessing a trigonal arrangement in the molecule $\text{CH}_3\text{B}(\text{OH})_2$, thus giving a tetrahedral O_3BC group—or the molecule of this boronic acid forms the corresponding diester with 7, which undergoes a following deprotonation. Both the above pathways shown in Scheme S1 (see Supplementary Materials) seem to be the probable chemical transformation. Indeed, the pK_{a1} value for methylboronic acid and those for the initial α -dioximes H_2Nx and H_2Ox , which have been measured in aqueous solutions, are known from the literature [30–33] to be almost equal and to fall in the ranges 10.4–10.7 [30,31], 10.6 [33] and 10.5–10.7 [32], respectively. So, at the maximal concentrations of the corresponding α -dioximes and $\text{CH}_3\text{B}(\text{OH})_2$ equal to 3×10^{-3} and 3×10^{-1} mol L⁻¹, respectively, and pH = 3.75, those of their monoanionic forms do not exceed 5×10^{-10} and 7×10^{-8} mol L⁻¹, while the initial concentration of Fe^{2+} ions is close to 10^{-5} mol L⁻¹. Moreover, dissociation of their molecules in mixed aqueous–organic media should be even lower. On the other hand, the non-macrocyclic metal oximate complexes typically possess substantially lower pK_a values than the initial

oximes [34]. So, under the used experimental conditions, the proposed pathway of a given multistep chemical transformation shown in Scheme 3 is substantially more probable than that based on a formation of the monoanionic form of $\text{CH}_3\text{B}(\text{OH})_2$ as the first stage (see Supplementary Materials, Scheme S1). Finally, the semiclathrocholate intermediate **8** formed can easily undergo a multistage cross-linking with the second molecule of methylboronic acid as a Lewis-acidic capping agent with elimination of H^+ ion and two water molecules (see the discussion above), thus giving the dimethylboron-capped macrobicyclic molecule $\text{FeOx}_3(\text{BCH}_3)_2$ (**5**) that possesses a distorted TP quasiaromatic cage framework (see below for its XRD structure). So, as follows from Scheme 3, which is in good agreement with the obtained experimental data, there are three main stages which determine the overall rate of the formation of this clathrocholate molecule.



Scheme 3. Plausible pathway of a formation of the clathrocholate $\text{FeOx}_3(\text{BCH}_3)_2$ (**5**).

2.3. X-ray Structures

Trying to explain the above differences in the kinetics of a formation of the clathrocholate analogs $\text{FeNx}_3(\text{BCH}_3)_2$ (**4**) and $\text{FeOx}_3(\text{BCH}_3)_2$ (**5**)—the derivatives of six- and eight-membered alicyclic α -dioximate ligand synthons—we performed the single crystal XRD study of their molecular structures. The latter were compared with known X-ray structures of the initial α -dioximes [35] and that of their *n*-butylboron-capped tris-octoximate analog $\text{FeOx}_3(\text{Bn-C}_4\text{H}_9)_2$ [5].

General views of the molecules $\text{FeOx}_3(\text{BCH}_3)_2$ (**5**) and $\text{FeNx}_3(\text{BCH}_3)_2$ (**4**) are shown in Figures 8 and 9, respectively; the main geometrical parameters of their clathrocholate frameworks and those for their *n*-butylboron- and adamantylboron-capped analogs are listed in Tables 2 and 3. These tables also contain the direct XRD data for the molecules of the initial alicyclic α -dioximes. In the former macrobicyclic molecules, the encapsulated iron(II) ion is situated in the center of its FeN_6 -coordination polyhedron possessing the geometry intermediate between a TP and a TAP; the values of φ for these methylboron-capped tris- α -dioximate clathrochelates are equal to 26.0 and 18.9°, respectively. As can be seen from Tables 2 and 3, the φ values for *n*-butylboron- and adamantylboron-capped iron(II) tris-octoximates [5,36] are higher than those for their tris-nioximate analogs, while other geometrical parameters of their macrobicyclic frameworks are very similar. In particular, the averaged Fe–N distances in all these molecules are close to 1.90 Å, thus they are characteristic of the macrobicyclic iron(II) tris- α -dioximates [1,2], and their oligo- and

polymeric derivatives [37–49] as well, which are reported to be the diamagnetic compounds. Indeed, Fe–N distances in the high-spin iron(II) complexes, the derivatives of *N*-donor ligands, are typically higher than 2.0 Å [50,51].

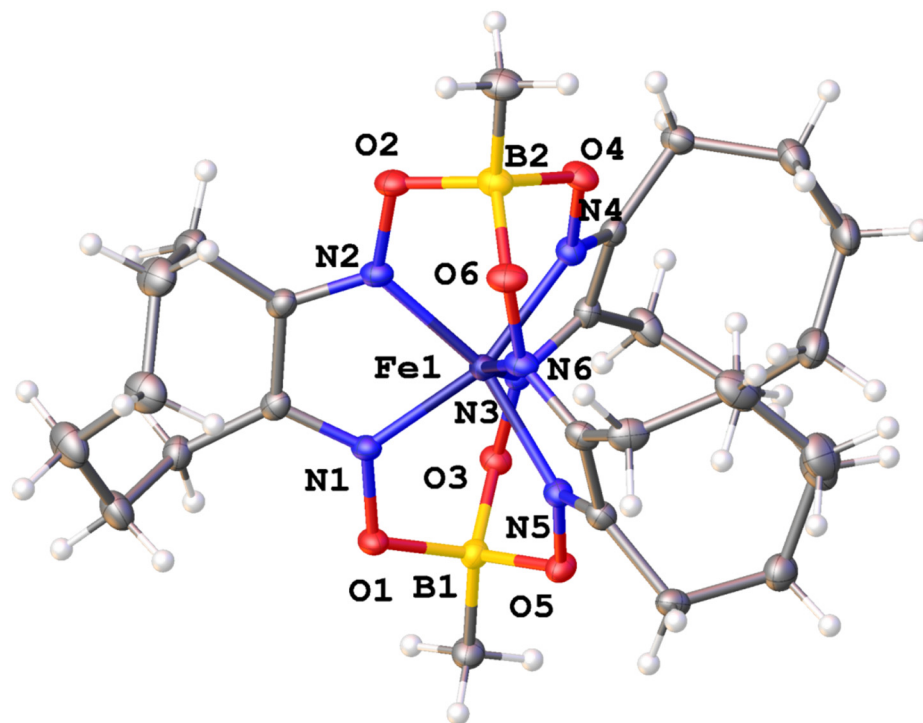


Figure 8. General view of the molecule FeO₃(BCH₃)₂ (5) in representation of its atoms with thermal ellipsoids ($p = 50\%$).

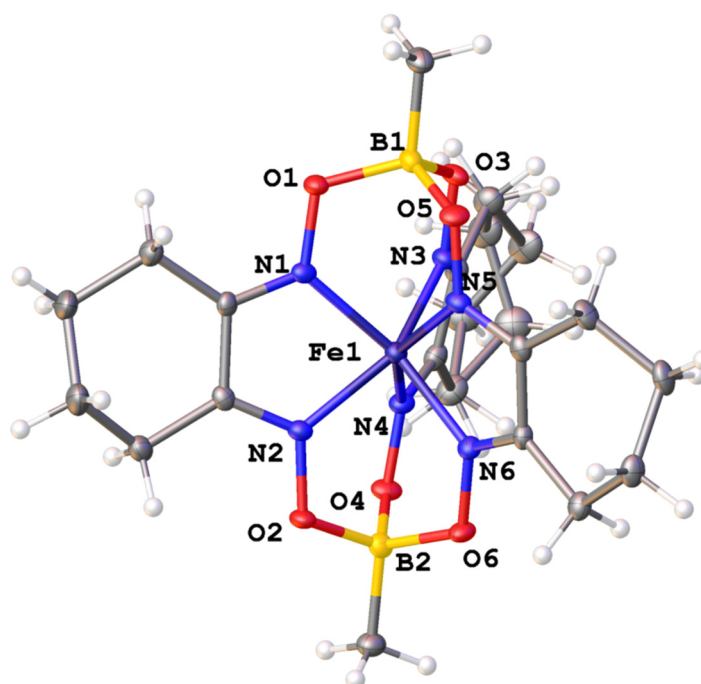


Figure 9. General view of the molecule FeN_x₃(BCH₃)₂ (4) in representation of its atoms with thermal ellipsoids ($p = 50\%$).

Table 2. Main geometrical parameters of the alkylboron-capped iron(II) tris-octoximate molecules and those for initial α -dioxime (octoxime).

Parameter	^a FeOx ₃ (BCH ₃) ₂ (5)	FeOx ₃ (B <i>n</i> -C ₄ H ₉) ₂ [5]	^b FeOx ₃ (BAd) ₂ [36]	H ₂ Ox [35]
Fe–(Å)	1.910(2)–1.921(2) av. 1.916	1.868(11)–1.929(11) av. 1.895	1.895(2)–1.911(2) av. 1.899	-
B–O (Å)	1.512(3)–1.526(3) av. 1.519	1.497(19)–1.510(20) av. 1.505	1.495(4)–1.515(4) av. 1.502	-
N–O (Å)	1.387(2)–1.394(2) av. 1.390	1.363(13)–1.394(10) av. 1.375	1.366(3)–1.383(3) av. 1.375	1.409(2)–1.413(4) av. 1.411
C=N (Å)	1.315(3)–1.323(2) av. 1.318	1.28(2)–1.34(2) av. 1.314	1.289(4)–1.313(4) av. 1.303	1.291(3)–1.293(7) av. 1.292
chelate C–C (Å)	1.460(3)–1.463(3) av. 1.461	1.439(16)–1.459(17) av. 1.445	1.440(5)–1.454(5) av. 1.447	1.492(7)
^c N . . . N (Å)	2.432(2)–2.436(3) av. 2.434	2.387(12)–2.412(14) av. 2.397	2.401(4)–2.408(4) av. 2.405	2.667(3)
N=C–C=N (°)	av. 6.8	av. 5.7	av. 6.2	26.6(6)
φ (°)	26.0	25.1	25.2	
α (°)	78.8	78.4	78.6	
h (Å)	2.34	2.31	2.31	

^a This work. ^b “Ad” means an adamantyl residue. ^c “N . . . N” means the distance between two nitrogen atoms of the same α -dioximate ligand fragment.

Table 3. Main geometrical parameters of the alkylboron-capped iron(II) tris-nioximate molecules and those for the initial α -dioxime (nioxime).

Parameter	^a FeNx ₃ (BCH ₃) ₂ (4)	FeNx ₃ (B <i>n</i> -C ₄ H ₉) ₂ [52]	^b FeNx ₃ (BAd) ₂ [36]	H ₂ Nx [35]
Fe–N (Å)	1.911(2)–1.918(2) av. 1.914	1.895(3)–1.923(3) av. 1.911	1.898(2)–1.906(2) av. 1.902	
B–O (Å)	1.498(3)–1.513(3) av. 1.503	1.466(5)–1.532(5) av. 1.504	1.499(3)–1.506(3) av. 1.503	
N–O (Å)	1.372(2)–1.379(2) av. 1.376	1.368(3)–1.386(3) av. 1.376	1.365(2)–1.374(2) av. 1.369	1.402(3)–1.410(3) av. 1.406
C=N (Å)	1.302(3)–1.314(3) av. 1.308	1.295(5)–1.325(4) av. 1.309	1.304(3)–1.308(2) av. 1.306	1.276(3)–1.280(3) av. 1.278
C–C (Å)	1.435(3)–1.446(3) av. 1.440	1.414(4)–1.441(4) av. 1.428	1.432(2)–1.439(3) av. 1.436	1.489(3)
^c N . . . N (Å)	2.420(2)–2.424(3) av. 2.421	2.402(3)–2.427(3) av. 2.414	2.413(3)–2.425(2) av. 2.417	2.682(3)
N=C–C=N (°)	av. 6.5	av. 7.6	av. 6.0	26.2(2)
φ (°)	18.9	21.1	22.9	
α (°)	78.4	78.4	79	
h (Å)	2.37	2.35	2.34	

^a This work. ^b “Ad” means an adamantyl residue. ^c “N . . . N” means the distance between two nitrogen atoms of the same α -dioximate ligand fragment.

A relative rigidity of the π -conjugated diazomethine fragment N=C–C=N in the molecules of all alicyclic α -dioximes disfavors an ability of cyclohexane fragment of the initial nioxime molecule and those of its tris- α -dioximate clathrochelate derivatives to adopt its(their) *chair* or *boat* conformation(s). As a result, this(these) alicyclic fragment(s) adopt(s) a *twist* conformation in all cage molecules of this type with known X-ray structures, and in the molecule H₂Nx as well. The average deviations of carbon atoms in its(their) six-membered alicyclic fragment(s) from the corresponding mean plain(s) do not exceed 0.10–0.13 Å (Figure 10, top). At the same time, its(their) structural lability causes a disordering of two α -carbon atoms of this six-membered alicycle, which are inherently bound to the above N=C–C=N fragment, into two crystallographically independent positions (i.e., the

presence of two different *twist* conformations). Such a disordering is observed not only in the molecule $\text{FeN}_x\text{}_3(\text{BCH}_3)_2$ (4), but also in the X-rayed [53] co-crystals of nioxime with 4,4'-bipyridine and with 1,2-bis(4-pyridyl)ethane, as well as in the molecules of other boron-capped iron(II) tris-nioximates with known X-ray structures [1,5]. Despite the fact that the formation of a macrobicyclic framework does not affect the conformations of their alicyclic ribbed substituents, the presence of bulky aliphatic substituents at their capping boron atoms causes the substantial changes in the angles $\text{C}=\text{N}-\text{O}$ and $\text{N}=\text{C}-\text{C}=\text{N}$ in a rigid polyazomethine cage framework, and a shortening of the chelate $\text{C}-\text{C}$ bonds as well (Table 2). At the same time, with other bond distances, valent and torsion angles in their macrobicyclic frameworks are characteristic of the corresponding structural elements, as follows from the "Mogul geometry check" treatments, which were implemented within the Mercury package [54].

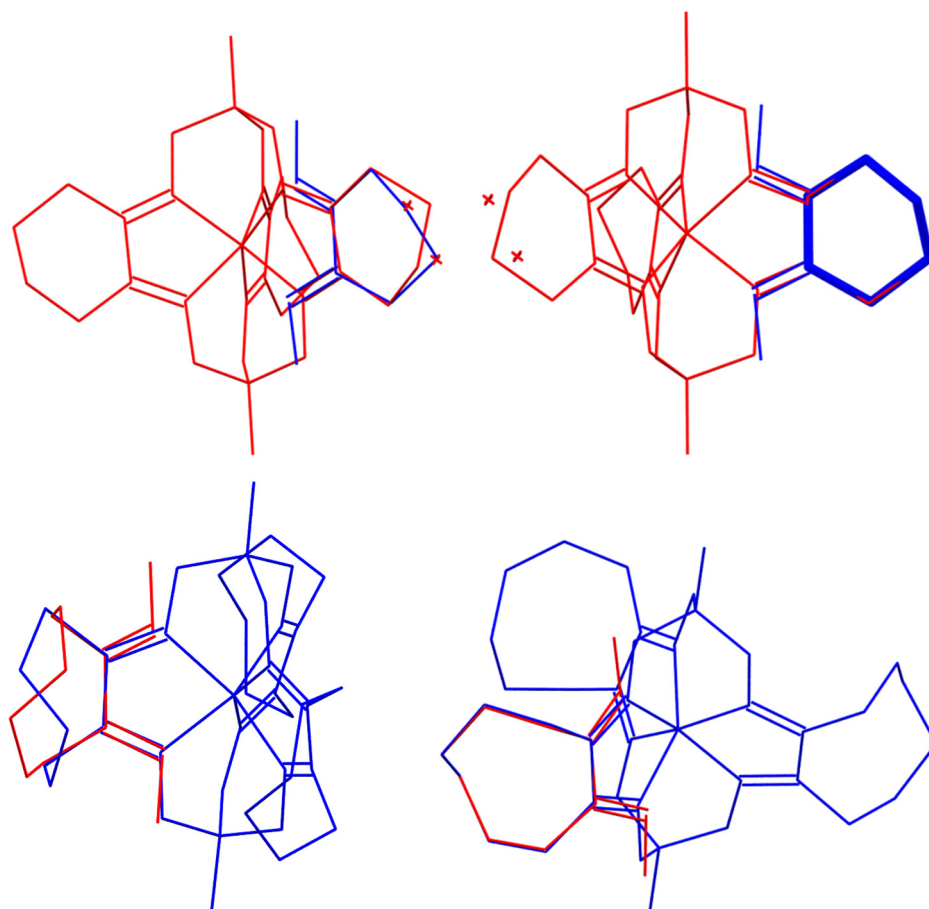


Figure 10. Comparison of a geometry of cyclohexane (on top) and cyclooctane (on bottom) alicyclic fragments in the corresponding boron-capped iron(II)-encapsulating clathrochelate molecules and the initial α -dioximes.

It seems to be quite unexpected that, despite a big number of the rotational degrees of freedom in the case of an eight-membered alicyclic moiety, it adopts a *boat-chair* conformation (see Figure 10, bottom). The latter is fully ordered both in the initial molecule of octoxime [35], and in those of its clathrochelate derivatives with known X-ray structures (this work, [5,36]). Moreover, all these cage molecules, listed in Table 3, possess the very similar whole conformations: two of their three eight-membered alicyclic ribbed substituents are positioned close to each other (Figure 11). The changes in the mutual positions of oxygen, nitrogen and carbon atoms in the chains $\text{O}-\text{N}=\text{C}-\text{C}=\text{N}-\text{O}$ of the molecule $\text{FeOx}_3(\text{BCH}_3)_2$ (5), caused by their coordination to the encapsulated iron(II) ion, are similar to those for its tris-nioximate analogs. On the other hand, the average changes in the

positions of carbon atoms of two cyclooctane rings of this molecule with respect to the molecule of initial α -dioxime are close to 0.05\AA only, the third alicyclic fragment of this type underwent a complete inversion of its conformation, as compared with H_2Ox . This effect can be caused by the formation of intramolecular interactions between two bulky neighboring eight-membered rings; the stabilization of an overall conformation of the molecule $\text{FeOx}_3(\text{BCH}_3)_2$ (5) requires an adoption of the above fully inverted conformation for one of its three cyclooctane ribbed substituents (Figure 11).

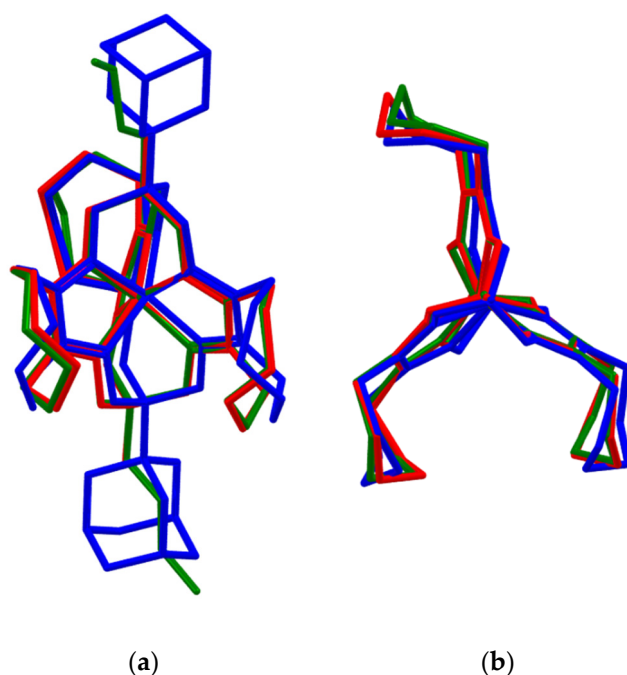


Figure 11. Superposition of the side (a) and top (b) views of the molecules $\text{FeOx}_3(\text{BCH}_3)_2$ (5, shown in red), $\text{FeOx}_3(\text{Bn-C}_4\text{H}_9)_2$ (shown in green) and $\text{FeOx}_3(\text{BAd})_2$ (shown in blue) used for their comparison. Hydrogen atoms are omitted for clarity. Their main superimposed atoms are Fe1, B1, B2 and six nitrogen atoms as well.

Thus, the observed differences in the kinetics and the schemes of a formation of the hydroxyboran- and methylboron-capped iron(II) tris-nioximates,—the derivatives of six-membered alicyclic α -dioxime—on the one hand, and those of their tris-octoximate analogs—the derivatives of eight-membered alicyclic ligand synthons—on the other hand, can be explained using the above direct XRD data. In the latter cases, the substantial structural changes of the geometry of their chelating ligand synthons, caused by their coordination to the encapsulated iron(II) ion are necessary. They can also result from a higher distortion of its TAP-TP FeN_6 -coordination polyhedron (and, therefore, that of a quasiaromatic cage framework), as well as from the intramolecular non-covalent interactions and sterical clashes of their bulky ribbed substituents in the molecules of the boron-capped macrobicyclic tris-octoximates. All these factors cause the substantial changes in the ratios between the rates of the multistep initial stages of these multistage template reactions, thus affecting their kinetic and thermodynamic parameters and their overall schemes as well (including the number of main stages which affect the overall synthesis reaction rate).

2.4. Acidic Decomposition of $\text{FeOx}_3(\text{BCH}_3)_2$ in Its Diluted Solutions

The acidic decomposition rate constants k_{eff}^d for the initially prepared complex $\text{FeOx}_3(\text{BCH}_3)_2$ (5) were also obtained as the pseudo-first-order rate constants (Equation (15)), but with respect to the concentration of this clathrochelate:

$$\ln A = k_{eff}^d t \quad (15)$$

An example of the determination of this constant is shown in Figure 12. The values of the decomposition reaction rate constants k_{eff}^d were obtained as the tangents of linear regressions plotted in the coordinates $\ln A$ versus time.

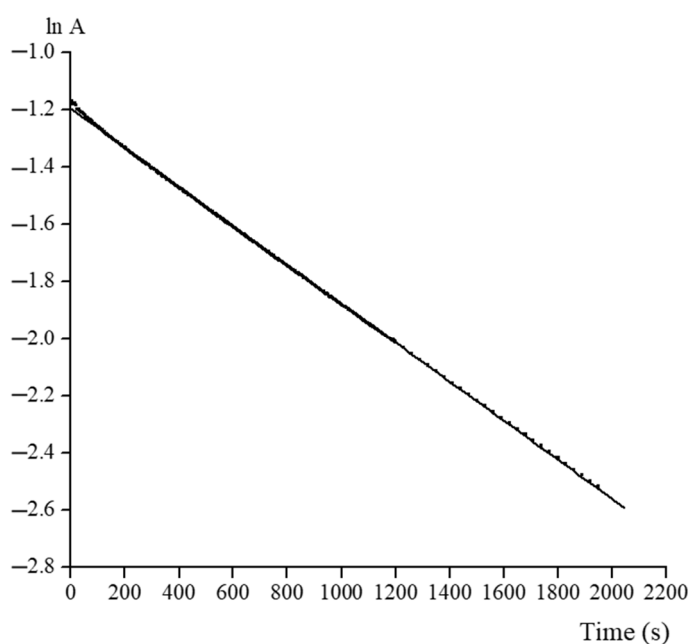


Figure 12. Example of a determination of the decomposition reaction rate constant k_{eff}^d for the clathrochelate $\text{FeOx}_3(\text{BCH}_3)_2$ (5) at its concentration $4.6 \times 10^{-5} \text{ mol L}^{-1}$ in 2.6 M solution of sulfuric acid ($a_{H^+} = 0.019 \text{ mol L}^{-1}$).

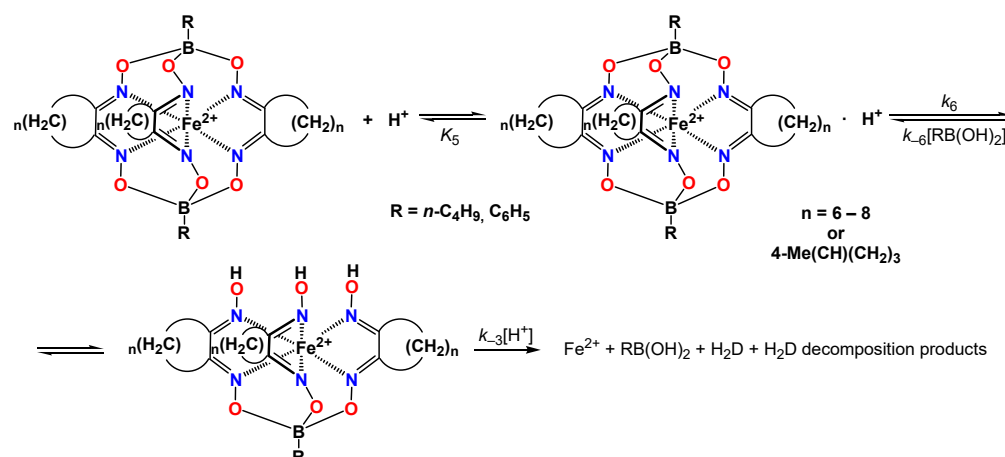
Decomposition of the *n*-butyl- and phenylboron-capped iron(II) alicyclic tris-dioximates clathrochelates is known from literature [1,4,5,36] requiring their protonation (Scheme 4). The corresponding apical substituents cannot be protonated under these experimental conditions and H^+ ions add to the ester oxygen atoms of the B–O–N chains of their capping fragment exclusively in the strongly acidic media. The following stepwise cleavage of the boron-containing capping groups and the protonation of the intermediate products lead to the irreversible decomposition of a given clathrochelate molecule. The addition of great amount of the corresponding boronic acid substantially increases the rate of reverse cross-linking process on the second stage of this decapping reaction, thus causing a decrease in its rate.

When the rates of the individual stages of this decomposition are deduced to be equal (i.e., the concentrations of its intermediates are constant), Scheme 4 can be described using the following equations:

$$-d[\text{complex}]/dt = k_{-3}[\text{Fe}(\text{HD})_3(\text{BR})^+] a_{H^+} \quad (16)$$

$$-d[\text{complex}]/dt = k_6[\text{FeD}_3(\text{BR})_2 \cdot \text{H}^+] - k_{-6}[\text{Fe}(\text{HD})_3(\text{BR})^+][\text{RB}(\text{OH})_2] \quad (17)$$

$$K_5 = \frac{[\text{FeD}_3(\text{BR})_2 \cdot \text{H}^+]}{[\text{FeD}_3(\text{BR})_2] a_{H^+}} \quad (18)$$



Scheme 4. Most plausible pathway of the acidic decomposition of the *n*-butyl- and phenylboron-capped iron(II) alicyclic tris- α -dioximates. Adapted from [1].

Since the changes in an optical density are caused by destruction of all of the colored complex forms shown in Scheme 4, their total concentration can be written as follows:

$$[\text{complex}] = [\text{Fe}(\text{HD})_3(\text{BR})_2] + [\text{Fe}(\text{HD})_3(\text{BR})_2 \cdot \text{H}^+] + [\text{Fe}(\text{HD})_3(\text{BR})^+] \quad (19)$$

So, the decomposition effective rate constant can be described as:

$$k_{eff}^d = \frac{k_{-3}k_6K_5a_{H^+}^2}{k_{-3}a_{H^+} + k_{-6}[\text{RB}(\text{OH})_2] + k_{-3}K_5a_{H^+}^2 + k_{-6}K_5a_{H^+}[\text{RB}(\text{OH})_2] + k_6K_5a_{H^+}} \quad (20)$$

This enables one to determine the values of the corresponding constants or those of their ratios. In the absence of the corresponding boronic acid and in harsh acidic media, the amounts of $k_{-6}[\text{RB}(\text{OH})_2]$ and of $K_5k_{-6}a_{H^+}[\text{RB}(\text{OH})_2]$ become negligible, as compared with those of other components of this equation, and k_{eff}^d can be expressed as:

$$k_{eff}^d = \frac{k_{-3}k_6K_5a_{H^+}^2}{k_{-3}a_{H^+} + k_6K_5 + k_{-3}K_5a_{H^+}} \quad (21)$$

Acidic decomposition of the cage iron(II) complexes under study both in the absence and in the presence of methylboronic acid (Figures 13 and 14) could not be described by the above Equations (20) and (21). As can be seen from Figure 14, the values of k_{eff}^d for the complexes $\text{FeN}_x\text{O}_3(\text{BCH}_3)_2$ (4) and $\text{FeO}_x\text{O}_3(\text{BCH}_3)_2$ (5) in the absence of methylboronic acid are almost the same up to the activity of H^+ ions of approximately 0.035 mol L^{-1} . On the other hand, its further increase resulted in a substantial difference between them (up to $30 \div 40\%$ at the a_{H^+} values in the range $0.13\text{--}0.15 \text{ mol L}^{-1}$). Indeed, the corresponding k_{eff}^d values for the tris-octoximate clathrochelate $\text{FeO}_x\text{O}_3(\text{BCH}_3)_2$ (5) go up substantially slower than those for its tris-nioximate analog $\text{FeN}_x\text{O}_3(\text{BCH}_3)_2$ (4). The addition of methylboronic acid caused a substantial decrease in the rates of their acidic decomposition (Figure 14), but this effect is more pronounced in the case of the complex $\text{FeO}_x\text{O}_3(\text{BCH}_3)_2$ (5) than that for its homolog $\text{FeN}_x\text{O}_3(\text{BCH}_3)_2$ (4). In particular, at the concentration of methylboronic acid equal to $3.06 \times 10^{-2} \text{ mol L}^{-1}$, the difference in the rates of the acidic decomposition of $\text{FeO}_x\text{O}_3(\text{BCH}_3)_2$ (5) in the absence and in the presence of this capping agent is $0.3\text{--}0.4 \times 10^{-3} \text{ s}^{-1}$ (approximately 30–50%). The same effect for its tris-nioximate analog was observed at the concentration of methylboronic acid equal to 0.153 mol L^{-1} . This suggests a substantial difference in the rates of the corresponding capping–decapping reactions.

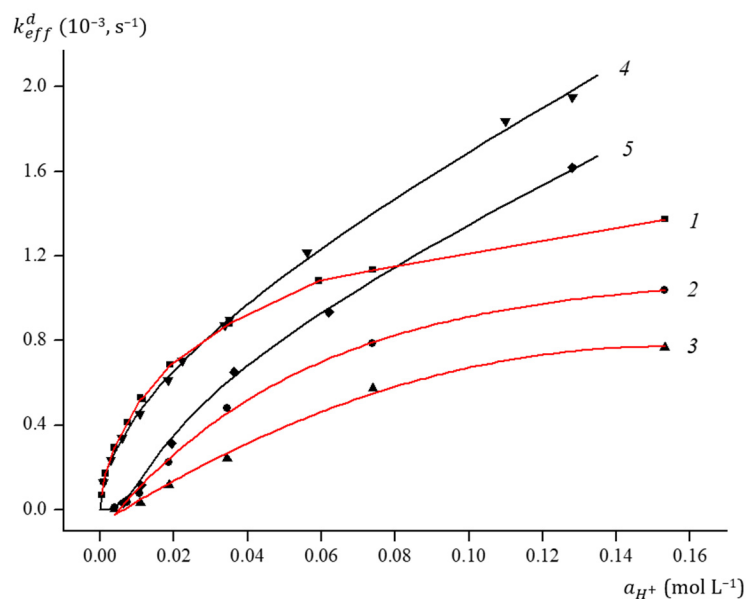


Figure 13. Plots of the k_{eff}^d values for clathrochelates $\text{FeOx}_3(\text{BCH}_3)_2$ (5, this work, shown in red, at the concentrations of methylboronic acid equal to 0 (1), 3.06×10^{-2} (2) and 6.38×10^{-2} (3) mol L^{-1}) and $\text{FeNx}_3(\text{BCH}_3)_2$ (4, shown in black, at the concentrations of methylboronic acid equal to 0 (4) and 1.53×10^{-1} (5) mol L^{-1}) versus the activity of H^+ ions. Adapted from ref. [6].

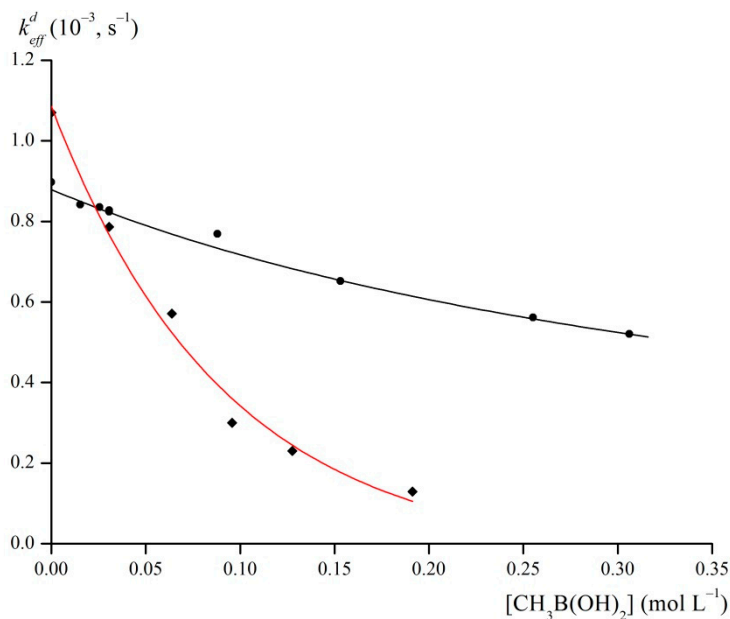


Figure 14. Plots of k_{eff}^d of the acidic decomposition of clathrochelates $\text{FeOx}_3(\text{BCH}_3)_2$ (this work, 5, shown in red) and $\text{FeNx}_3(\text{BCH}_3)_2$ (4, shown in black) versus the concentration of methylboronic acid at the activities of H^+ ions equal to 7.39×10^{-2} and 3.62×10^{-2} mol L^{-1} , respectively. Adapted from ref. [6].

Moreover, we studied an effect of the addition of this Lewis-acidic capping agent on the decomposition of $\text{FeOx}_3(\text{BCH}_3)_2$ (5). At the concentrations of $\text{CH}_3\text{B}(\text{OH})_2$ higher than approximately 0.19 mol L^{-1} (at the activity of H^+ ions equal to $7.39 \times 10^{-2} \text{ mol L}^{-1}$), the order of a given reaction with respect to the concentration of the initially obtained complex $\text{FeOx}_3(\text{BCH}_3)_2$ (5) substantially increases, and this process already cannot be described using the known [29] pseudo-first-order kinetic equation.

So, the following general Equation (22), describing all the obtained photometrical experimental data, was evaluated for the kinetics of the acidic decomposition of this cage complex versus the concentration of methylboronic acid and the activity of H^+ ions as well:

$$k_{eff}^d = \frac{a_{H^+}^2}{(E \cdot a_{H^+} + D \cdot a_{H^+} \cdot [CH_3B(OH)_2] + C \cdot a_{H^+}^{-0.5}) \cdot [CH_3B(OH)_2] + B \cdot a_{H^+}^2 + A \cdot a_{H^+}^{1.3}} \quad (22)$$

where $E = 345$, $D = 12.3 \times 10^3$, $C = 3.33$, $B = 549$ and $A = 55.7$.

For a more clear comparison, the earlier-evaluated [6] analogous equation for its homolog $FeNx_3(BCH_3)_2$ (4) was transformed into the following form:

$$k_{eff}^d = \frac{a_{H^+}^2}{E a_{H^+} + (D \cdot a_{H^+} + C \cdot a_{H^+}^{-1}) \cdot [CH_3B(OH)_2] + B \cdot a_{H^+}^2 + A \cdot a_{H^+}^{1.5}} \quad (23)$$

where $E = 1.41$, $D = 70$, $C = 3 \times 10^{-3}$, $B = -160.4$ and $A = 237.8$.

The presence in Equation (22), describing of the decomposition reaction of $FeOx_3(BCH_3)_2$ (5), of the integer second order on the concentration of methylboronic acid allows us to suggest that the detachment of the second molecule of $CH_3B(OH)_2$ in harsh acidic media is also a reversible process. However, as with the case of its clathrochelate analog $FeNx_3(BCH_3)_2$ (4), the presence of a fractional order with respect to the activity of H^+ ions in this equation suggests the absence of its physical meaning. It is probable that at least two parallel pathways of its acidic decomposition, which are affected by addition of $CH_3B(OH)_2$, proceed under our experimental conditions.

3. Experimental

3.1. Synthesis

3.1.1. Materials and Methods

The reagents used for the synthesis of a new clathrochelate complex under study, $FeCl_2 \cdot 4H_2O$ (Sigma-Aldrich[®], St. Louis, MO, USA), methylboronic acid (Acros[®], Tokyo, Japan), sorbents and organic solvents (Sigma-Aldrich[®]) were obtained commercially. Cyclooctanedion-1,2-dioxime (octoxime) was prepared by oxidation of cyclooctanone with SeO_2 and the obtained alicyclic eight-membered α -diketone was treated with hydroxylamine [3]. The complex $FeNx_3(BCH_3)_2$ (4) was obtained as described elsewhere [6]; its NMR and mass spectra are shown in (see Supplementary Materials, Figures S5–S7).

Analytical data (C, H, N contents) were obtained with a Carlo Erba model 1106 microanalyzer.

MALDI-TOF mass spectrum of the clathrochelate $FeOx_3(BCH_3)_2$ (Figure S8) was recorded with and without the matrix using a MALDI-TOF-MS Bruker Autoflex II (Bruker Daltonics) mass spectrometer in reflecto-mol mode. The ionization was induced by UV-laser with wavelength 337 nm. The sample was applied to a nickel plate, and 2,5-dihydroxybenzoic acid was used as the matrix. The accuracy of measurements was 0.1%.

1H and $^{13}C\{^1H\}$ NMR spectra of the complex $FeOx_3(BCH_3)_2$ (5) shown in Figures S9 and S10 were recorded from its CD_2Cl_2 solution with a Bruker Avance 600 spectrometer. The measurements were carried out using the residual signals of this deuterated solvent.

UV-Vis spectrum of its solution in dichloromethane was recorded in the range 250–800 nm with a Varian Cary 100 spectrophotometer.

3.1.2. Synthesis and Spectral Characteristics

$FeOx_3(BCH_3)_2$ (5). Octoxime (0.22 g, 1.32 mmol) and $FeCl_2 \cdot 4H_2O$ (0.08 g, 0.40 mmol) were dissolved in ethanol (3 mL) and the reaction mixture was stirred for 10 min. Then methylboronic acid (0.05 g, 0.88 mmol) and ethanol (1 mL) were added and the reaction mixture was stirred for 2 h at r.t. The orange precipitate formed was filtered off, washed with ethanol (20 mL, in four portions) and extracted with dichloromethane (10 mL). The

extract was filtered and chromatographically separated on silica gel (30-mm layer, eluent: dichloromethane). The first major red-orange elute was collected, filtered, the filtrate was evaporated to dryness, washed with hexane and dried in vacuo. Yield: 0.16 g (65 %). Found (%): C, 50.88; H, 7.02; N, 13.54. Calc. for $C_{26}H_{42}N_6B_2FeO_6$ (%): C, 51.02; H, 6.92; N, 13.73. MS(MALDI-TOF): m/z : 612 $[M]^+$. 1H NMR (CD_2Cl_2 , δ , ppm): -0.04 (br s, 6H, BCH_3), 1.35 (br s, 12H, γ - CH_2), 1.63 (br s, 12H, β - CH_2), 2.92 (br t, $J_{1H-1H} = 6$ Hz, 12H, α - CH_2). $^{13}C\{^1H\}$ NMR (CD_2Cl_2 , δ , ppm): 25.83 (s, γ - CH_2), 26.48 (s, β - CH_2), 28.47 (s, α - CH_2), 156.89 (s, C=N).

3.1.3. Single Crystal X-ray Diffraction Experiments

Single crystals of the complexes $FeNx_3(BCH_3)_2$ (**4**) and $FeOx_3(BCH_3)_2 \cdot CH_2Cl_2$ (**5**· CH_2Cl_2) were grown from their saturated solutions in chloroform:ethanol 1:10 and dichloromethane:heptane 1:3 mixtures, respectively. The intensities of reflections were measured with a Bruker Apex II CCD diffractometer using Mo-K α radiation of a graphite monochromator ($\lambda = 0.71073$ Å). The structures were solved using the SHELXTL algorithm [55] and refined by full-matrix least squares against F^2 . Non-hydrogen atoms were refined in an anisotropic approximation; the positions of the H(C) atoms were calculated. All hydrogen atoms were included in a refinement by the riding model with $U_{iso}(H) = nU_{eq}(X)$, where $n = 1.5$ for hydrogen atoms of methyl groups and 1.2 for other hydrogen atoms. All calculations were made using the SHELXL-2015 [56] and OLEX2 [57] program packages. The crystallographic parameters and the refinement details for the above X-rayed single crystals are listed in Table S1 (see Supplementary Materials).

CCDCs 2,036,146 and 2,036,147 contain the supplementary crystallographic data for this paper. These data can be obtained free of charge via <http://www.ccdc.cam.ac.uk/structures>, accessed on 18 May 2021.

3.2. Kinetic Studies

3.2.1. Materials and Methods

The commercial $FeSO_4 \cdot 7H_2O$ (ACS Reagent, Sigma-Aldrich[®]), methylboronic acid (Acros[®]) and H_2SO_4 (Acros[®]) were used for the kinetic experiments; octoxime was obtained as described above. Bidistilled water and the additionally re-distilled ethanol and chloroform were used as the solvents for preparation of the reaction mixtures.

The initial reagents are almost optically silent in the visible range (see Supplementary Materials, Figure S4). So, kinetics of the template synthesis of $FeOx_3(BCH_3)_2$ (**5**) and that of its acidic decomposition were studied using the photometric measurements at a maximum of the corresponding intense MLCT band ($\lambda_{max} = 450$ nm) with a Cary-50 UV-vis spectrophotometer equipped with a thermostated 1×1 -cm quartz cell. Kinetic plots for both the synthesis and the acidic decomposition reactions of this macrobicyclic iron(II) tris-octoximate were evaluated using the “Kinetics” program package for the above spectrophotometer. The a_{H^+} values for the diluted slightly acidic solutions were obtained using a Sartorius PP-20 pH-meter equipped with PY-P11 pH-electrode. The obtained kinetic data were evaluated using the Excel and Origin Pro program packages.

3.2.2. Kinetic Experiments

Cage iron(II) complex $FeOx_3(BCH_3)_2$ (**5**) was formed in the quantitative yield in the diluted water-ethanol-chloroform mixture at 25 °C. The diluted aqueous solutions of $FeSO_4 \cdot 7H_2O$ and sulfuric acid were mixed with those of methylboronic acid and octoxime in ethanol for studying of kinetics of its synthesis. Chloroform (10 vol.%) was also added to increase solubility of this complex in a given solvent mixture. In all cases, the water:ethanol:chloroform v/v ratio was 3:6:1.

Kinetics of the acidic decomposition of the initially obtained clathrochelate $FeOx_3(BCH_3)_2$ (**5**) was studied using its solution in the same solvent mixture. A weighted amount of this complex, prepared as described above, was dissolved in a given volume of ethanol:chloroform 6:1 v/v mixture. Acidic decomposition experiments both in the absence and in

the presence of methylboronic acid were performed using a bulk 13.3 ÷ 13.5M aqueous H₂SO₄ solution.

Decomposition of the complex FeOx₃(BCH₃)₂ (5) proceeds within a reasonable time interval only in the strongly acidic media. Thus, the activities of H⁺ ions at high concentrations of H₂SO₄, as a source of these ions, in a given water–ethanol–chloroform mixture should be used in the corresponding kinetic and thermodynamic calculations. That is why we used the so-called “acidity function” H₀ = −log a_{H⁺}, the graphical presentation of which is plotted [6]; it has been earlier obtained [58] using an indicator method with *ortho*- and *para*-nitroanilines as UV-vis indicators in the same mixture at the same concentrations of H₂SO₄.

4. Conclusions

Thus, we unexpectedly found the dramatic effect of a ring size (six- versus eight-membered alicyclic substituents) of the chelating α-dioximate ligand synthons on the plausible kinetic scheme and thermodynamic parameters of the reactions of template assembly of their methylboron-capped iron(II)-encapsulating clathrochelate derivatives in the diluted aqueous–organic solutions. This factor also affects the rates of their decomposition in harsh acidic media. To explain the obtained results of the experimental solution photometric studies, we performed the single crystal XRD experiments for both these diamagnetic iron(II) clathrochelates and compared their results with known XRD structures of the initial alicyclic six- and eight-membered α-dioximes and those of their clathrochelate derivatives. This allowed us to deduce the structural reasons of the above substantial changes in the kinetics and thermodynamics of the synthesis and decomposition reactions of the macrobicyclic iron(II) compounds under study. The difference in the kinetic schemes of a formation of these alicyclic cage complexes was explained by necessity of the substantial changes in a geometry of the octoximate chelate fragments, caused by their coordination to the iron(II) ion, due to both the higher distortion of the FeN₆-coordination polyhedra, and the intramolecular sterical clashes in the molecules of the macrobicyclic iron(II) tris-octoximates.

Supplementary Materials: The following materials are available online, Table S1. Crystallographic parameters and the experimental details for the X-rayed single crystals of the methylboron-capped alicyclic tris-α-dioximates FeNx₃(BCH₃)₂ and FeOx₃(BCH₃)₂·CH₂Cl₂. Scheme S1. Probable alternative pathways of a formation of the clathrochelate FeOx₃(BCH₃)₂ (5). Figures S1–S4. Plots of linear regressions for determination of various kinetic constants. Figures S5–S10. The experimental NMR and mass spectra for the above cage complexes, and the discussion about their spin state.

Author Contributions: Synthesis of the clathrochelate complexes (A.S.B.); performing of kinetic experiments (A.L.P.); treatment and discussion of kinetic data (Y.Z.V.); evaluation and discussion of the XRD structures (A.V.V.); performing and discussion of UV-vis experiments (E.G.L.); performing and discussion of NMR and MS experiments (I.G.B.); supervision, writing and editing of the paper (Y.Z.V.). All authors have read and agreed to the published version of the manuscript.

Funding: The synthesis of cage complex was supported by Russian Science Foundation (project 21-73-20145). A.S.B. also thanks the financial support of the Russian Foundation for Basic Research (grant 20-03-00127). The spectral part was performed in a framework of the IGIC RAS state assignment in the field of basic scientific researches. X-ray diffraction data were performed with the financial support from Ministry of Science and Higher Education of the Russian Federation using the equipment of Center for molecular composition studies of INEOS RAS. MALDI-TOF mass spectrometric measurements were performed using an equipment of CKP FMI IPCE RAS.

Data Availability Statement: Data available in a publicly accessible repository.

Conflicts of Interest: The authors declare no conflict of interest.

Sample Availability: Samples of the compounds are not available from the authors.

References

1. Voloshin, Y.Z.; Kostromina, N.A.; Krämer, R. *Clathrochelates: Synthesis, Structure and Properties*; Elsevier: Amsterdam, The Netherlands, 2002.
2. Voloshin, Y.; Belaya, I.; Krämer, R. *Cage Metal Complexes: Clathrochelates Revisited*; Springer: Berlin/Heidelberg, Germany, 2017.
3. Voloshin, Y.Z.; Noskov, Y.G. Kinetics of the template synthesis and decomposition of iron(II) macrobicyclic hydroxy-boron-containing cyclooctandione-1,2-dioximate. *Ukr. Khim. Zh.* **1993**, *59*, 347–352.
4. Voloshin, Y.Z.; Noskov, Y.G.; Terekhova, M.I.; Kron, T.E. The influence of the substituent and ring size on the kinetic and thermodynamic parameters of template synthesis and decomposition reaction of clathrochelate alkyl- and aryl-boron-containing iron(II) tris-dioximates. *Pol. J. Chem.* **1996**, *70*, 1229–1235.
5. Voloshin, Y.Z.; Terekhova, M.I.; Noskov, Y.G.; Zavodnik, V.E.; Belsky, V.K. Structure aspects of kinetics and thermodynamics of the template synthesis and decomposition reactions of boron-containing clathrochelate iron(II) dioximates. *An. Quim. Int.* **1998**, *94*, 142–147.
6. Pomadchik, A.L.; Belov, A.S.; Lebed, E.G.; Voloshin, Y.Z. Kinetics and Thermodynamics of the Template Synthesis and of an Acidic Decomposition of the Clathrochelate Iron(II) Tris-Cyclohexanedion-1,2-Dioximate (Nioximate) Formed by a Cross-Linking with Methylboronic Acid. *Russ. J. Inorg. Chem.* **2020**, *65*, 1503–1512. [[CrossRef](#)]
7. Wang, Y.-M.; Chung, C.-S.; Lo, J.-M.; Wu, Y.-L. Kinetics and mechanism of the complexation reaction of copper(II) with diazadioximes. *Polyhedron* **1999**, *18*, 1917–1925. [[CrossRef](#)]
8. Biver, T.; Secco, F.; Tinè, M.R.; Venturini, M. Equilibria and kinetics of complex formation between copper(II) and the polyamine Me2octaen. *Polyhedron* **2001**, *20*, 1953–1959. [[CrossRef](#)]
9. Stynes, D.; Vernik, I.; Zobi, F. Iron complexes of borylated vicinal dioxime macrocycles. *Coord. Chem. Rev.* **2002**, *233–234*, 273–287. [[CrossRef](#)]
10. Sharma, V.; Millero, F.J.; Homonnay, Z. The kinetics of the complex formation between iron(III)–ethylenediaminetetraacetate and hydrogen peroxide in aqueous solution. *Inorg. Chim. Acta* **2004**, *357*, 3583–3587. [[CrossRef](#)]
11. Biver, T.; Secco, F.; Tinè, M.R.; Venturini, M. Kinetics and equilibria for the formation of a new DNA metal-intercalator: The cyclic polyamine Neotrien/copper(II) complex. *J. Inorg. Biochem.* **2004**, *98*, 33–40. [[CrossRef](#)] [[PubMed](#)]
12. Ozay, H.; Baran, Y. Synthesis, complex formation kinetics and thermodynamic study of some acyclic polyamine and N2O2 ligands with copper(II). *J. Coord. Chem.* **2010**, *63*, 4299–4308. [[CrossRef](#)]
13. Nandi, D.; Chattopadhyay, A.; Ray, S.; Acharjee, A.; Sarkar, R.; Laskar, S.; Ghosh, A.K. Kinetic and mechanistic studies on the substitution of aqua ligands from diaquaethylenediamineplatinum(II) ion by vicinal dioximes. *Mon. Chem. Chem. Mon.* **2015**, *147*, 1015–1022. [[CrossRef](#)]
14. Parker, B.F.; Zhang, Z.; Rao, L.; Arnold, J. An overview and recent progress in the chemistry of uranium extraction from seawater. *Dalton Trans.* **2017**, *47*, 639–644. [[CrossRef](#)]
15. Jackels, S.C.; Rose, N.J. Encapsulation reactions. Synthesis and characterization of clathrochelates derived from iron(II), dimethylglyoxime and boron compounds. *Inorg. Chem.* **1973**, *12*, 1232–1237. [[CrossRef](#)]
16. Voloshin, Y.Z.; Polshin, E.V.; Nazarenko, A.Y. Prediction of the Geometry of Low-Spin Iron(II) Complexes Using a Modified Concept of Partial Quadrupole Splitting (PQS): Advantages and Limitations. *Hyperfine Interact.* **2002**, *141/142*, 309–320. [[CrossRef](#)]
17. Asher, R.L.; Stevens, J.G. A Mössbauer spectroscopic investigation of a series of boron-capped iron II clathrochelates. *J. Solid State Chem.* **1990**, *87*, 408–414. [[CrossRef](#)]
18. Nagy, L.; Zsákó, J.; Novak, C.; Várhelyi, C.; Vanko, G.; Liptay, G. On the Oximine Complexes of Transition Metals: Part 110: Spectroscopic and DSC study on some [Fe(Diox·H)2L2] and [Fe(Diox)3(BOR)2] type chelates and clathrochelates. *J. Therm. Anal. Calorim.* **1999**, *57*, 433–445. [[CrossRef](#)]
19. Lever, A.B.P. *Inorganic Electronic Spectroscopy*, 2nd ed.; Elsevier: Amsterdam, The Netherlands, 1984.
20. Kepert, D.L. *Inorganic Stereochemistry*; Springer: Berlin/Heidelberg, Germany, 1982.
21. Bancroft, G. Partial quadrupole splittings in inorganic chemistry. *Coord. Chem. Rev.* **1973**, *11*, 247–262. [[CrossRef](#)]
22. Bancroft, G.M. *Mössbauer Spectroscopy—An Introduction for Inorganic Chemists and Geochemists*; McGraw-Hill: New York, NY, USA, 1973.
23. Dabrowiak, J.C.; Merrell, P.H.; Stone, J.A.; Busch, D.H. Mössbauer spectra of iron complexes with macrocyclic ligands. Partial center shifts and partial quadrupole splittings. *J. Am. Chem. Soc.* **1973**, *95*, 6613–6622. [[CrossRef](#)]
24. Kuzmann, E.; Lengyel, A.; Homonnay, Z.; Várhelyi, C.; Klencsár, Z.; Kubuki, S.; Szalay, R. Mössbauer study of novel iron(II)-dioxime complexes with branched alkyl chains. *Hyperfine Interact.* **2014**, *226*, 181–185. [[CrossRef](#)]
25. Larsen, E.; LaMar, G.N.; Wagner, B.E.; Parks, J.E.; Holm, R.H. Three-dimensional macrocyclic encapsulation reactions. III. Geometrical and electronic features of tris(diimine) complexes of trigonal-prismatic, antiprismatic, and intermediate stereochemistry. *Inorg. Chem.* **1972**, *11*, 2652–2668. [[CrossRef](#)]
26. Sato, H.; Tominaga, T. Mössbauer Studies of the Thermal Decomposition of Tris(2,2'-bipyridine)iron(II) Chloride and the Structures of the Isomers of 2,2'-Bipyridineiron(II) Chloride. *Bull. Chem. Soc. Jpn.* **1976**, *49*, 697–700. [[CrossRef](#)]
27. Linert, W.; Gutmann, V.; Wiesinger, G.; Perkins, P.G. CNDO/2-MO Calculations and Mössbauer Spectroscopy on Tris-(1,10-Phenanthroline)iron-Complexes. *Z. Phys. Chem.* **1984**, *142*, 221–238. [[CrossRef](#)]

28. Vargas, A.; Hauser, A.; Daku, L.M.L. Influence of Guest–Host Interactions on the Structural, Energetic, and Mössbauer Spectroscopy Properties of Iron(II)tris(2,2′-bipyridine) in the Low-Spin and High-Spin States: A Density-Functional Theory Study of the Zeolite-Y Embedded Complex. *J. Chem. Theory Comput.* **2009**, *5*, 97–115. [[CrossRef](#)]
29. Schmid, R.; Sapunov, V.N. *Non-Formal Kinetics*; Verlag Chemie: Weinheim, Germany, 1982.
30. Babcock, L.; Pizer, R. Dynamics of boron acid complexation reactions. Formation of 1:1 boron acid-ligand complexes. *Inorg. Chem.* **1980**, *19*, 56–61. [[CrossRef](#)]
31. Haines, R.A.; Ryan, D.E.; Cheney, G.E. 5-methyl-1,2,3-cyclohexanetrionetroxime: A comparative study with some vic-dioximes. *Can. J. Chem.* **1962**, *40*, 1149–1159. [[CrossRef](#)]
32. Finta, Z.; Mitrache, I.; Várhelyi, C.; Zsako, J.; Horák, J. Acidity constants of 1,2-cycloheptane- and 1,2-cyclo-octanedione dioximes. *Microchim. Acta* **1979**, *71*, 405–413. [[CrossRef](#)]
33. Banks, C.V.; Carlson, A.B. Determination of acidic dissociation constants of several vic-dioximes. *Anal. Chim. Acta* **1952**, *7*, 291–301. [[CrossRef](#)]
34. Gómez-Tagle, P.; Lugo-González, J.C.; Yatsimirsky, A.K. Oximate metal complexes breaking the limiting esterolytic reactivity of oximate anions. *Chem. Commun.* **2013**, *49*, 7717–7719. [[CrossRef](#)]
35. Streltsova, N.R.; Bel'Sky, V.K.; Voloshin, Y.Z. Structures of three alicyclic α -dioximes with a ring size of six to eight. *Acta Crystallogr. Sect. C Cryst. Struct. Commun.* **1993**, *49*, 635–639. [[CrossRef](#)]
36. Voloshin, Y.; Varzatskii, O.A.; Belov, A.; Lebedev, A.Y.; Makarov, I.S.; Gurskii, M.E.; Antipin, M.Y.; Starikova, Z.A.; Bubnov, Y.N. Cage iron(II) complexes with apical and ribbed adamantyl substituents: The creation of second (hydrophobic) shell of an encapsulated metal ion. *Inorg. Chim. Acta* **2007**, *360*, 1543–1554. [[CrossRef](#)]
37. Wise, M.D.; Ruggi, A.; Pascu, M.; Scopelliti, R.; Severin, K. Clathrochelate-based bipyridyl ligands of nanoscale dimensions: Easy-to-access building blocks for supramolecular chemistry. *Chem. Sci.* **2013**, *4*, 1658–1662. [[CrossRef](#)]
38. Wise, M.D.; Holstein, J.J.; Pattison, P.; Besnard, C.; Solari, E.; Scopelliti, R.; Bricogne, G.; Severin, K. Large, heterometallic coordination cages based on ditopic metallo-ligands with 3-pyridyl donor groups. *Chem. Sci.* **2014**, *6*, 1004–1010. [[CrossRef](#)]
39. Jansze, S.M.; Cecot, G.; Wise, M.D.; Zhurov, K.O.; Ronson, T.K.; Castilla, A.M.; Finelli, A.; Pattison, P.; Solari, E.; Scopelliti, R.; et al. Ligand Aspect Ratio as a Decisive Factor for the Self-Assembly of Coordination Cages. *J. Am. Chem. Soc.* **2016**, *138*, 2046–2054. [[CrossRef](#)] [[PubMed](#)]
40. Jansze, S.M.; Wise, M.D.; Vologzhanina, A.V.; Scopelliti, R.; Severin, K. PdII2L4-type coordination cages up to three nanometers in size. *Chem. Sci.* **2016**, *8*, 1901–1908. [[CrossRef](#)] [[PubMed](#)]
41. Cecot, G.; Marmier, M.; Geremia, S.; De Zorzi, R.; Vologzhanina, A.V.; Pattison, P.; Solari, E.; Tirani, F.F.; Scopelliti, R.; Severin, K. The Intricate Structural Chemistry of MII2nLn-Type Assemblies. *J. Am. Chem. Soc.* **2017**, *139*, 8371–8381. [[CrossRef](#)] [[PubMed](#)]
42. Jansze, S.M.; Cecot, G.; Severin, K. Reversible disassembly of metallasupramolecular structures mediated by a metastable-state photoacid. *Chem. Sci.* **2018**, *9*, 4253–4257. [[CrossRef](#)]
43. Jansze, S.M.; Ortiz, D.; Tirani, F.F.; Scopelliti, R.; Menin, L.; Severin, K. Inflating face-capped Pd6L8 coordination cages. *Chem. Commun.* **2018**, *54*, 9529–9532. [[CrossRef](#)]
44. Jansze, S.M.; Severin, K. Palladium-Based Metal–Ligand Assemblies: The Contrasting Behavior upon Addition of Pyridine or Acid. *J. Am. Chem. Soc.* **2019**, *141*, 815–819. [[CrossRef](#)]
45. Bila, J.L.; Pijeat, J.; Ramorini, A.; Fadaei-Tirani, F.; Scopelliti, R.; Baudat, E.; Severin, K. Porous networks based on iron(ii) clathrochelate complexes. *Dalton Trans.* **2019**, *48*, 4582–4588. [[CrossRef](#)]
46. Cecot, G.; Doll, M.T.; Planes, O.M.; Ramorini, A.; Scopelliti, R.; Fadaei-Tirani, F.; Severin, K. Cages vs. Prisms: Controlling the Formation of Metallosupramolecular Architectures with Ligand Side-Chains. *Eur. J. Inorg. Chem.* **2019**, *2019*, 2972–2976. [[CrossRef](#)]
47. Planes, O.M.; Jansze, S.M.; Scopelliti, R.; Fadaei-Tirani, F.; Severin, K. Two-Step Synthesis of Linear and Bent Dicarboxylic Acid Metalloligands with Lengths of up to 3 nm. *Inorg. Chem.* **2020**, *59*, 14544–14548. [[CrossRef](#)]
48. Planes, O.M.; Schouwink, P.A.; Bila, J.L.; Fadaei-Tirani, F.; Scopelliti, R.; Severin, K. Incorporation of Clathrochelate-Based Metalloligands in Metal–Organic Frameworks by Solvent-Assisted Ligand Exchange. *Cryst. Growth Des.* **2020**, *20*, 1394–1399. [[CrossRef](#)]
49. Sudan, S.; Li, R.-J.; Jansze, S.M.; Platzeck, A.; Rudolf, R.; Clever, G.H.; Fadaei-Tirani, F.; Scopelliti, R.; Severin, K. Identification of a Heteroleptic Pd6L6L'6 Coordination Cage by Screening of a Virtual Combinatorial Library. *J. Am. Chem. Soc.* **2021**, *143*, 1773–1778. [[CrossRef](#)]
50. Legrand, V.; Pillet, S.; Weber, H.-P.; Souhassou, M.; Létard, J.-F.; Guionneau, P.; LeComte, C. On the precision and accuracy of structural analysis of light-induced metastable states. *J. Appl. Crystallogr.* **2007**, *40*, 1076–1088. [[CrossRef](#)]
51. Pillet, S.; Legrand, V.; Weber, H.-P.; Souhassou, M.; Létard, J.-F.; Guionneau, P.; Lecomte, C. Out-of-equilibrium charge density distribution of spin crossover complexes from steady-state photocrystallographic measurements: Experimental methodology and results. *Z. Krist. Cryst. Mater.* **2008**, *223*, 235–249. [[CrossRef](#)]
52. Voloshin, Y.Z.; Varzatskii, O.A.; Belov, A.; Starikova, Z.A.; Strizhakova, N.G.; Dolganov, A.V.; Kochubey, D.I.; Bubnov, Y.N. Synthesis, X-ray structure and redox properties of the macrobicyclic iron(II) N2- and S2-containing vic-dioximates. *Inorg. Chim. Acta* **2010**, *363*, 134–146. [[CrossRef](#)]

53. Coropceanu, E.B.; Croitor, L.; Siminel, A.V.; Chumakov, Y.; Fonari, M.S. The luminescence attenuation in the solid state by fluoride anion entrapped in the one-dimensional Zn(II) dioximate and mononuclear Cd(II) dioxime compounds. *Polyhedron* **2016**, *109*, 107–114. [[CrossRef](#)]
54. Macrae, C.F.; Sovago, I.; Cottrell, S.J.; Galek, P.T.A.; McCabe, P.; Pidcock, E.; Platings, M.; Shields, G.P.; Stevens, J.S.; Towler, M.; et al. Mercury 4.0: From visualization to analysis, design and prediction. *J. Appl. Crystallogr.* **2020**, *53*, 226–235. [[CrossRef](#)]
55. Sheldrick, G.M. SHELXT—Integrated space-group and crystal-structure determination. *Acta Crystallogr. Sect. A Found. Adv.* **2015**, *71*, 3–8. [[CrossRef](#)]
56. Sheldrick, G.M. Crystal structure refinement with SHELXL. *Acta Cryst.* **2015**, *71*, 3–8.
57. Dolomanov, O.V.; Bourhis, L.J.; Gildea, R.J.; Howard, J.A.K.; Puschmann, H. OLEX2: A complete structure solution, refinement and analysis program. *J. Appl. Cryst.* **2009**, *42*, 339–341. [[CrossRef](#)]
58. Voloshin, Y.Z.; Noskov, Y.G. Kinetics of template synthesis and decomposition of butyl- and phenyl-boron-containing clathrochelate tris-nioximates of iron(II). *Ukr. Khim. Zh.* **1993**, *59*, 231–235.